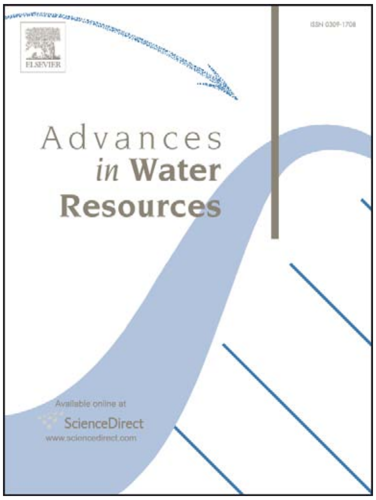

Effect of mineral reactions on the hydraulic properties of unsaturated soils: Model development and application

L. Wissmeier, D.A. Barry

PII: S0309-1708(09)00075-X
DOI: 10.1016/j.advwatres.2009.05.004
Reference: ADWR 1421

To appear in: *Advances in Water Resources*

Received Date: 13 August 2008
Revised Date: 29 April 2009
Accepted Date: 7 May 2009

Please cite this article as: Wissmeier, L., Barry, D.A., Effect of mineral reactions on the hydraulic properties of unsaturated soils: Model development and application, *Advances in Water Resources* (2009), doi: 10.1016/j.advwatres.2009.05.004

Effect of mineral reactions on the hydraulic properties of unsaturated soils: Model development and application

L. Wissmeier* and D.A. Barry

Ecole Polytechnique Fédérale de Lausanne (EPFL)
Institut d'Ingénierie de l'Environnement
Laboratoire de Technologie Ecologique
CH-1015 Lausanne, Switzerland

Resubmitted on 29 April 2009 to Advances in Water Resources

---

*Author to whom all correspondence should be addressed. Telephone: +41 21 693 5727, facsimile: +41 21 693 5670.
E-mail addresses: laurin.wissmeier@epfl.ch (L. Wissmeier), andrew.barry@epfl.ch (D.A. Barry).

Abstract

The *selective radius shift* model was used to relate changes in mineral volume due to precipitation/dissolution reactions to changes in hydraulic properties affecting flow in porous media. The model accounts for (i) precipitation/dissolution taking place only in the water-filled part of the pore space and further that (ii) the amount of mineral precipitation/dissolution within a pore depends on the local pore volume. The pore bundle concept was used to connect pore-scale changes to macroscopic soil hydraulic properties. Precipitation/dissolution induces changes in the pore radii of water-filled pores and, consequently, in the effective porosity. In a time step of the numerical model, mineral reactions lead to a discontinuous pore-size distribution because only the water-filled pores are affected. The pore-size distribution is converted back to a soil moisture characteristic function to which a new water retention curve is fitted under physically plausible constraints. The model equations were derived for the commonly used van Genuchten/Mualem hydraulic properties. Together with a mixed-form solution of Richards' equation for aqueous phase flow, the model was implemented into the geochemical modelling framework PHREEQC, thereby making available PHREEQC's comprehensive geochemical reactions. Example applications include kinetic halite dissolution and calcite precipitation as a consequence of cation exchange. These applications showed marked changes in the soil's hydraulic properties due to mineral precipitation/dissolution and the dependency of these changes on water contents. The simulations also revealed the strong influence of the degree of saturation on the development of the saturated hydraulic conductivity through its quadratic dependency on the van Genuchten parameter α. Furthermore, it was shown that the unsaturated hydraulic conductivity at fixed reduced water content can even increase during precipitation due to changes in the pore-size distribution.

Keywords: Dissolution; Precipitation; Reactive solute transport; PHREEQC; Mualem; Van Genuchten; Moisture content; Hydraulic conductivity; Vadose zone; Pore bundle model; Selective radius shift model; Split operator; Water retention; Soil moisture characteristic; Young-Laplace law; Halite; Cation exchange

1 Introduction

Due to the importance of the unsaturated zone as a buffer zone for aquifers against contamination, the simulation of geochemical reactions together with vadose zone flow and solute transport is receiving increasing interest. Some of the more advanced computer programs that have emerged in recent years are MULTIFLO [1], FLOTRAN [2], MIN3P [3], TOUGHREACT [4] and HP1 [5]. In order to model hydro-geochemical and ecological engineering problems they employ continuum representations of the porous medium [6-9] and assume the existence of a representative elementary volume where, for instance, flow can be described by Darcy's law. However, geochemical reactions such as mineral dissolution/precipitation (hereafter termed simply mineral reactions) modify the porous medium's pore structure. These changes manifest themselves in the constitutive relations that characterize the continuum-scale properties of the soil and are used in the governing equations of flow and transport. An up-scaling procedure has to be employed in order to treat pore-scale interactions of the fluid and the solid soil structure within the framework of continuum flow and transport models [10-13].

Existing approaches that account for continuum-scale hydraulic property changes due to biological activity or mineral reactions include statistical grain size analysis [14], discrete description of mineral geometries [15] and estimates of changes in pore-size distributions (PSD's) [16-18]. In these models, the effects of mineral reactions on constitutive relations are considered for saturated conditions. That is, the only hydraulic property that is changed is the saturated hydraulic conductivity. On the other hand, in unsaturated porous media, there are two hydraulic properties governing flow, the soil moisture characteristic curve and the unsaturated conductivity [e.g., 8]. Because pore-scale mineral reactions alter the shape and volume of water-filled pores, in consequence both these properties have to be adapted.

In a recent modelling study on reactive solute transport Cochepin et al. [19] highlight "(...) the importance of properly describing and simulating the way the texture evolves in porous medium (sic) when porosity undergoes significant variations." In this work, we present a model that integrates pore-scale effects of mineral dissolution and precipitation, namely changes in pore volume, into continuum-scale simulations of unsaturated flow, transport and geochemical reactions. The pore bundle or capillary tube concept [20-27] is employed to relate bulk changes in mineral volumes to PSD's and thereby to soil moisture characteristic curves.

Fig. 1 describes schematically our modelling approach: Starting with continuum-scale hydraulic properties, the PSD is calculated from the soil moisture characteristic curve using the pore bundle concept. Changes in mineral volume through equilibrium or kinetic mineral reactions are translated to changes in pore radii of the PSD according to the *selective radius shift* model (described below). The resulting new PSD is converted back to an updated soil moisture characteristic curve, which is then used for computing flow and transport at the continuum scale.

Fig. 1 near here

The module for updating the PSD with changes in mineral volume is based on the film approach by Taylor et al. [18], which assesses the effect of bacterial growth on flow and transport in saturated porous media. The authors state that the extension of their model to the case of unsaturated flow is straightforward. Nevertheless, Saripalli et al. [28] remarked, in a review on changes in hydrologic properties of aquifer media due to chemical reactions, that no research has been done on this topic in unsaturated soils. In order to fill this knowledge gap Freedman et al. [29] adapted the Taylor model to simulate the effect of mineral reactions in partially saturated soils. Even though they recognized that mineral reactions may occur only in the smaller, water-filled pores of the pore-size spectrum, the effect of liquid phase saturation is neglected in their model. Here, we address this issue using the *selective radius shift* model wherein the influence of reactions between the aqueous and mineral phases in unsaturated porous media is limited to the water-filled pore space. Other important features of the model are:

- Modifications of pore radii through mineral reactions according to the volume of water in the pore (which limits the possible amount of mineral reaction); and
- Precise treatment of changes in analytical PSD’s without prior discretisation into pore-size classes.

The model is implemented through the geochemical modelling framework PHREEQC [30], into which a 1D solution of unsaturated flow and transport has been integrated. In developing the model in PHREEQC, the full set of geochemical reactions and connected thermodynamic databases are accessible. This allows for the simulation of numerous applied hydro-geochemical environmental engineering problems where mineral reactions have an important influence on the physical properties of partially saturated soils. Possible applications include vadose zone biodegradation processes [31,32], water management practices and irrigation techniques in arid and semiarid areas [33-35], salinity management [36-39] and the assessment of the long-term performance of reactive barriers [40-46].

Below, we present the theoretical model derivation followed by applications of the model to the case of kinetic halite dissolution in different moisture conditions and calcite precipitation due to cation exchange.

2 Theory

In the model the governing continuum-scale equations for 1D unsaturated flow (Richards' equation) and solute transport (advection-dispersion equation) are solved using the numerical scheme of Celia et al. [47] and the simplified total variation diminishing scheme of Gupta et al. [48].

In contrast to most common simulators for unsaturated flow and multi-species solute transport [4,5,49], our scheme represents liquid phase flow through a consequent application of solute transport to all elements in the solution including oxygen and hydrogen. This results in mass conservative computation of liquid phase flow together with an accurate representation of pH [50].

The governing equations for equilibrium solution speciation, heterogeneous phase reactions (e.g., mineral dissolution/precipitation, cation exchange and surface adsorption) and kinetic reactions are described in the PHREEQC user manual [30].

2.1 Pore bundle concept

The pore space of the soil is conceptualized as cylindrical capillaries with a continuous distribution of radii r (L). A given capillary can be either water-filled or completely dry, depending on the saturation state of the soil [23-26]. With this geometric idealization, the soil moisture characteristic curves $\theta(h)$ can be interpreted as continuous cumulative pore-size distributions, $\theta(r)$, by the Young-Laplace equation [e.g., 20,51-53]:

$$h = \frac{\zeta}{r}, \tag{1}$$

where h is the fluid pressure head (L) and θ is the volume of water-containing pores per unit volume of soil at a given pressure head. The capillarity factor ζ (L^2) is defined as:

$$\zeta = \frac{2\sigma \cos\phi}{\rho g}, \tag{2}$$

with surface tension of water σ (ML^2T^{-1}), contact angle between fluid and solid ϕ, fluid density (ML^{-3}) and magnitude of gravitational acceleration g (LT^{-2}) .

The cumulative PSD represents the relative volume of drainable pores with a radius equal to or smaller than r. In this paper, we assume a unique functional dependency of θ on h and therefore neglect hysteresis in the water retention. The drainable pore-size density function (or PSD) is obtained by differentiation of the cumulative PSD with respect to r [18,54]:

$$f(r) = \frac{d\theta(r)}{dr}. \tag{3}$$

Mineral reactions impose a change on PSD's through alterations of pore radii and, consequently, porosity. In the discretised time domain of a numerical model with a time step Δt, mineral reactions result in a finite change of pore space $\Delta\theta^m$, which is equal to the change in mineral volume with opposite sign.

With the given definition of θ, the saturated moisture content θ_{sat} is equal to the effective porosity. The new saturated moisture content, θ_{sat}^*, after Δt following mineral reaction is:

$$\theta_{sat}^* = \theta_{sat} + \Delta\theta^m = \int_0^\infty f^*(\eta)d\eta\,, \tag{4}$$

where f^* is the new PSD that results from modification of pore-radii and $\Delta\theta^m$ is known a priori from reaction calculations. The new cumulative pore volume, $\theta^*(r)$, is then given by:

$$\theta^*(r) = \int_0^r f^*(\eta)d\eta\,. \tag{5}$$

With the conceptualization of cylindrical pores whose length are not affected by mineral reactions, the new PSD can be calculated by substituting the transformed pore radii r^* into the original PSD Eq. (3) [18]:

$$f^*(r) = \frac{f(r^*)r^2}{{r^*}^2}. \tag{6}$$

Eq. (6) follows from the assumption that the number of pores in the system remains constant. The functional form of r^* is yet undefined and depends on the conceptualization of the simulated process. A constraint is imposed by Eq. (4), which states that the volume change due to changes in pore radii integrates to the total change in porosity.

As described earlier, the soil moisture characteristic curve is used to determine the soil's initial PSD. Any water retention curve can be used although here the *selective radius shift* model (§2.2) is applied to the commonly used van Genuchten soil moisture characteristic curve [55]:

$$\theta(h) = \theta_{res} + \frac{\theta_{sat} - \theta_{res}}{[1 + (\alpha h)^n]^m}, \tag{7}$$

with residual moisture content θ_{res} and parameters α (L^{-1}), n and $m = 1\text{-}\frac{1}{n}$. Therefore, the cumulative pore-volume per unit volume of soil is given by:

$$\theta(r) = \theta_{res} + \frac{\theta_{sat} - \theta_{res}}{\left[1 + \left(\alpha \frac{\zeta}{r}\right)^n\right]^m}, \tag{8}$$

and, following Eq. (3), the differential pore-volume becomes [17]:

$$f(r) = \frac{m\, n\, (\theta_{sat} - \theta_{res}) \left(\alpha \frac{\zeta}{r}\right)^n}{r\left[1 + \left(\alpha \frac{\zeta}{r}\right)^n\right]^{m+1}}. \tag{9}$$

2.2 Selective radius shift model

We assume a strict dependency of mineral reactions on solution concentrations, in other words that the amount of dissolved or precipitated mineral in a given pore is linearly dependent on its pore-volume. Consequently, , since we assume that the change in pore volume is uniform within a given pore, the accompanying radius change after a time step Δt is dependent on the pore radius at the start of the time step.

A dimensionless scalar proportionality factor relates the new and original pore radii in the PSD [cf., 18]:

$$r^* = \frac{r}{L_f}. \tag{10}$$

For cylindrical tubes of constant length a change in pore radius by a factor of L_f leads to a change in pore volume proportional to L_f^2. For dissolution $L_f > 1$ and for precipitation $L_f < 1$.

In a recent study [29], changes in mineral volume in unsaturated soils were modelled as affecting the entire pore spectrum despite that mineral reactions occur only in the water-filled part of the pore space. Here, instead, the *selective radius shift* model translates changes in mineral volumes to pore radii in the wet part of the porous medium.

In a given portion of the porous medium (in computational terms this would be a cell within the modelled domain), at any time the moisture content is known. Due to precipitation/dissolution, the pore volume will change and thus the soil moisture characteristic changes also. Thus, in the following we distinguish between the actual moisture content in the cell θ_{act}, and the moisture content as defined by the soil moisture characteristic curve. The maximum radius up to which pores are water-filled and therefore affected by mineral reactions is calculated from Eq. (8) with θ_{act} according to:

$$r_{lim} = \alpha\zeta \left[\left(-\frac{\theta_{sat} - \theta_{res}}{\theta_{act} + \theta_{res}} \right)^{\frac{1}{m}} - 1 \right]^{-\frac{1}{n}}. \tag{11}$$

The radius r_{lim} divides the pore spectrum into a dry, inert part and a wet reactive part, which has to compensate for the change in mineral volume. For the calculation of the new PSD, only the pore radii of the wet pore space are divided by the proportionality factor L_f.

Combining the PSD of the reaction affected wet part and the inert dry part leads to:

$$f^*(r) = f\left(\frac{r}{L_f}\right) L_f^2 \left[1 - \mathrm{H}\left(r - r_{lim} L_f\right)\right] + f(r)\mathrm{H}(r - r_{lim}), \tag{12}$$

where H is the Heaviside step function [e.g., 56]. Integration of Eq. (12) leads to the new cumulative pore volume, which is a piecewise discontinuous function:

$$\begin{aligned} \theta^*(r) = \theta_{res} &+ \frac{L_f^3(\theta_{sat} - \theta_{res})}{\left[1 + \left(\alpha\zeta \frac{L_f}{r}\right)^n\right]^m} \left[1 - \mathrm{H}\left(r - r_{lim} L_f\right)\right] \\ &+ L_f^3 \frac{(\theta_{sat} - \theta_{res})}{\left[1 + \left(\frac{\alpha\zeta}{r_{lim}}\right)^n\right]^m} \mathrm{H}\left(r - r_{lim} L_f\right) \\ &+ \left\{ \frac{\theta_{sat} - \theta_{res}}{\left[1 + \left(\frac{\alpha\zeta}{r}\right)^n\right]^m} - \frac{\theta_{sat} - \theta_{res}}{\left[1 + \left(\frac{\alpha\zeta}{r_{lim}}\right)^n\right]^m} \right\} \mathrm{H}(r - r_{lim}). \end{aligned} \tag{13}$$

The new saturated moisture content/effective porosity is

$$\lim_{r\to\infty} \theta^*(r) = \theta_{sat}^* = (\theta_{act} - \theta_{res}) \left(L_f^3 - 1\right) + \theta_{sat}. \tag{14}$$

Since the amount of mineral reaction is known in a time step, an explicit expression for L_f results:

$$L_f^3 = \left(\frac{\theta_{sat}^* - \theta_{sat}}{\theta_{act} - \theta_{res}}\right) + 1. \tag{15}$$

For the case of dissolution, the increase of pore radii in the wet part of the pore space leads to an overlap of PSD's of the wet and the dry pore space. This results from the fact that the wet pore space extends into the pore-size region of the dry pore space after an increase in pore radii. Precipitation produces a gap between wet and dry portions of the PSD. The underlying assumption is that water does not redistribute during reactions over a time step.

Fig. 2a shows the two separate PSD's for the dry, inert part of the pore space and the water-filled part after mineral reactions according to Eq. (12) together with the PSD that results from the procedure to fit the soil moisture characteristic curve (§3.2). The total pore volume is a combination of wet and dry pore volumes. The graph illustrates the overlap of the wet and dry PSD's in the pore-size interval $[r_{lim}, r_{lim}L_f]$ due to mineral dissolution in the water-filled portion only. The cumulative pore volume of the porous medium after mineral reactions is shown in part (b) of the graph, which was calculated with Eq. (25). Discontinuities resulting from the overlap of the two pore-size domains are identified by vertical lines.

In this example the initial PSD was derived from the van Genuchten soil moisture characteristic curve for loamy sand [57]. The pore radius that divides the water-filled and the dry pore spectrum r_{lim} is taken as 0.001 mm. This corresponds to a moisture content of 0.195. For illustrative purposes the L_f-factor is artificially magnified to a value of 1.2, which relates to an increase in effective porosity by 0.046 during a single time step Δt. This value is much larger than would occur in numerical simulations and was chosen simply to display how mineral reactions affect the PSD. In the example applications (§4, §6), the maximum change in effective porosity in a single time step is orders of magnitude smaller, which gives values of L_f closer to unity.

Fig. 2 near here

Fig. 3 shows the original water retention curve in terms of head together with the discontinuous piecewise soil moisture characteristics that results from Eq. (13). In addition, the fitted moisture characteristic curve that is used for the calculation of unsaturated aqueous phase flow is displayed. More details on the fitting procedure are given in §3.2.

Fig. 3 near here

2.3 Permeability model

From the numerous models that can be used to relate changes in hydraulic conductivity and mineral reactions to microbial activity [e.g., 17,22,58-65], the popular Mualem approach [66] was chosen for both relative conductivity and saturated conductivity, in order to be consistent with the underlying assumptions of the capillary pore bundle concept. The relative hydraulic conductivity K (LT^{-1}) is calculated from the saturated hydraulic conductivity K_{sat} (LT^{-1}) using:

$$K(\Theta) = K_{sat}\Theta^{l}\left[1-\left(1-\Theta^{\frac{1}{m}}\right)^{m}\right]^{2}, \tag{16}$$

where the reduced moisture content Θ, is defined by:

$$\Theta = \frac{\theta-\theta_{res}}{\theta_{sat}-\theta_{res}}, \tag{17}$$

and l is the tortuosity parameter.

Because of locally varying van Genuchten parameters as well as K_{sat}, the conductivity function becomes space and time dependent, i.e., at any location the conductivity evolves according to the local conditions, even if the initial soil is homogeneous. The new saturated conductivity after an incremental change in mineral volume is obtained from [18,54]:

$$K_{sat}^{*} = K_{sat}\left(\frac{\theta_{sat}^{*}}{\theta_{sat}}\right)^{l}\left[\frac{\int_0^{\infty}\frac{r^3}{r^{*2}}f^{*}(r)dr}{\int_0^{\infty}rf(r)dr}\right]^{2} = K_{sat}\left(\frac{\theta_{sat}^{*}}{\theta_{sat}}\right)^{l}\left[\frac{\alpha^{*}}{\alpha}\left(\frac{\theta_{sat}^{*}-\theta_{res}}{\theta_{sat}-\theta_{res}}\right)\right]^{2}, \tag{18}$$

where, as before, K_{sat}, α and θ_{sat} are the properties of the medium at the start of the time step and K_{sat}^{*}, α^{*} and θ_{sat}^{*} are the properties after time step Δt. Observe the independence of saturated conductivity of the shape parameter n, which is only true for $m = 1-\frac{1}{n}$ [17]. Limitations of this assumption were discussed by van Genuchten and Nielsen [67].

2.4 Mineral film model in saturated conditions

In fully saturated conditions where the entire PSD is affected by mineral reactions, the *selective radius shift* model reduces to a continuous film model. Eq. (13) becomes

$$\theta^{*}(h) = \frac{(\theta_{sat}-\theta_{res})L_f^3}{\left[1+\left(L_f\alpha h\right)^{n}\right]^{m}} + \theta_{res}, \tag{19}$$

where L_f is calculated from the change in mineral volume according to

$$L_f^3 = \left(\frac{\theta_{sat}^* - \theta_{res}}{\theta_{sat} - \theta_{res}}\right). \tag{20}$$

Due to the changes of pore radii in the entire PSD no fitting procedure has to be employed to determine the new soil moisture characteristic curve. As can be seen from Eq. (19), the parameter n is not affected by mineral reactions, whereas

$$\alpha^* = L_f \alpha. \tag{21}$$

In the fully saturated case, a comparison with the related biofilm model [18] can be performed. The Taylor model [18] assumes the development of an impermeable biofilm throughout the PSD with a homogeneous thickness, L_{fT} (L), irrespective of the pore volume according to

$$r^* = r + L_{fT}. \tag{22}$$

The change in pore radii affects the cumulative pore volume distribution as

$$\theta^*(r) = \int_0^r \frac{\eta^2}{(\eta + L_f)^2} f(\eta + L_{fT}) d\eta\,. \tag{23}$$

For the numerical integration of Eq. (23) in conjunction with the van Genuchten hydraulic model Maple version 12 [68] was used.

Fig. 4 near here

Fig. 4 shows the development of water retention curves in loamy sand [57] upon reduction in pore space by 20.2% according to the Taylor model [18] with a homogeneous film thickness ([18], Eq. (23)) and our model (Eq. (19)) where the film thickness is proportional to the pore volume. In the Taylor model [18], small pore sizes, characterized by larger drainage heads h, are equally affected by the clogging process, whereas our model shows an increasing reduction in pore size at lower drainage heads, which correspond to larger pores.

Fig. 5 near here

The development of hydraulic conductivity in relation to the pore space is illustrated in Fig. 5. A larger sensitivity of saturated conductivity on changes in pore volume is observed for our model compared to the Taylor model [18]. Since the large pore-size fraction carries most of the flow a reduction of its volume has a larger effect on conductivity than the same volume reduction in the small pore-size fraction. It is noted here that an analytical extension of the Taylor model

[18] to the case of dissolution is impeded by the singularity in the PSD at zero pore radius. Without additional assumptions, an additive increase in pore radii immediately leads to an infinite pore volume (see §7.2).

3 Numerical model description and implementation

3.1 Program flow

The numerical treatment of the simultaneous processes of aqueous phase flow and transport, reactions and changes in hydraulic properties was handled using, a sequential non-iterative split operator. The split operator decouples chemical element flow from geochemical speciation and reaction calculations as well as hydraulic parameter updating by solving sequentially in the discretised time domain. Extensive discussions of operator splitting techniques and their performance are available elsewhere [69-76].

Fig. 6 illustrates the split operator method used, with the main modules highlighted in bold. The variables that are passed between modules are shown in rounded boxes. At the beginning of every time step, aqueous phase flow and solute transport is calculated implicitly for all cells in the discretised spatial domain. Element concentrations are passed to the geochemical reaction calculations, which are carried out cell-wise. The change in mineral volume is passed to the hydraulic property model, which updates the hydraulic parameters of the current cell and saves them for use in the flow module in the following time step. Thus, flow calculations are performed globally for the entire domain whereas reactions and hydraulic parameter adjustments are calculated locally for each computational cell. With central finite differences for the space discretisation the accuracy of the computation of flow, transport and reactions is $\mathcal{O}(\Delta z^2, \Delta t)$.

Fig. 6 near here

The simulation of unsaturated flow and solute transport was extensively verified with HYDRUS-1D [77].

As mentioned above, the scheme was implemented through the modelling framework PHREEQC [30], which gives direct access to simulation of comprehensive geochemical processes. Solution speciation, cation exchange, surface adsorption and equilibrium mineral reactions are calculated according to standard thermodynamic models applying the local equilibrium assumption. Kinetic reactions are calculated by integrating user-definable rate equations.

The effect of reaction-induced changes in water contents (e.g., through mineral hydration, dissolution or precipitation) on flow, transport and hydraulic properties is *a priori* considered by re-calculating water contents from liquid phase elements after each reaction step.

3.2 Change in hydraulic parameters: Fitting procedure

The discontinuous PSD in Fig. 2a arises from the assumption that no redistribution of water is allowed during the reaction process. Although convenient, this is a somewhat crude approximation. Mineral reactions and water redistribution are simultaneous. Capillarity provides the mechanism to move water into the smallest pore-size fraction that can accommodate the current moisture content and therefore smooth the discontinuities in the PSD that are produced by the current conceptualization. For that reason, a new van Genuchten soil moisture characteristic curve is fitted to the piecewise retention function, Eq. (13), that results from pore-size-selective mineral reactions. The fitting procedure smoothes the small discontinuity in slope shown in Fig. 3. As well, there are significant practical benefits in fitting a unique soil moisture characteristic curve for every computational cell. It eliminates the need to (i) store a complex piecewise soil moisture characteristic curve, and (ii) to compute numerically the unsaturated hydraulic conductivity function (using Mualem's formula) for each computational cell at each time step.

For the simultaneous fitting of the van Genuchten parameters (n and α) a multidimensional downhill simplex method [78,79] was employed. Since Eq. (13) cannot be inverted analytically, the original soil moisture characteristic curve with θ_{sat}^{*} instead of θ_{sat} is evaluated at 40 locations equally distributed over the moisture spectrum from θ_{res} to θ_{sat}^{*}. (Tests have shown that a larger number of evaluation points does not yield noticeably improved fits.) The calculated values of h are inserted into Eq. (13) to yield 40 pairs of θ_i^{*} and h_i (full dots in Fig. 3) for which the new retention parameters n^{*} and a^{*} are optimized. The updated conductivity relation is then calculated based on the new retention parameters and Eq. (18).

The best fit for the new soil moisture characteristic curve calculated with a least-square objective function alone may predict a slight but unphysical increase of pore volumes in the dry part of the retention at precipitation and a decrease at dissolution. In order to prevent this non-physical behaviour, a penalty term is added to the least-square criterion in the overall objective function, σ:

$$\mathscr{o} = \sum_i \mathscr{r}_i^2 + |\mathscr{r}_i| \,\mathrm{H}\left[\mathscr{r}_{i-1} + \mathrm{sgn}\left(L_f - 1\right) \mathscr{r}_i\right] \left[1 - \mathrm{H}\left(h_i - \frac{\zeta}{r_{lim}}\right)\right] \times \left[1 - \mathrm{H}\left(h_i - \frac{\zeta}{r_{lim} L_f}\right)\right], \tag{24}$$

where sgn is the Sign function [e.g., 56]. In Eq. (24), $\mathscr{r}$ is the difference between the fitted Eq. (8) and Eq. (13) at the evaluation points i:

$$\mathscr{r}_i = \mathscr{r}(h_i) = \left\{\theta_{res} + \frac{\theta_{sat}^* - \theta_{res}}{\left[1 + (\alpha^* h_i)^{n^*}\right]^{1-\frac{1}{n^*}}}\right\} - \theta^*(h_i). \tag{25}$$

Because the endpoints of the retention curve (θ_{sat}^* and θ_{res}) are known, $\mathscr{r}_0 = 0$.

In words, Eq. (25) means that a penalty $|\mathscr{r}_i|$ is added for each evaluation point in the objective function, whose residual $\mathscr{r}_i$ is larger in the case of dissolution and smaller in case of precipitation compared to the previous evaluation point, counted in direction of increasing heads. In addition, the penalty is only applied if the head of the evaluation point is within the inert part of the pore spectrum. In the example from §2.2, the penalty ensures that the gradient of the fitted soil moisture characteristic in Fig. 3 is smaller than the gradient of $\theta^*(h)$, which results from Eq. (13) for heads smaller than $\frac{h_{lim}}{L_f}$. Looking at the PSD in Fig. 2a, the penalty guarantees that the PSD, which results from back-conversion of the fitted moisture characteristic always remains on or above $f(r)$ for the inert pore-size fraction.

Above it was noted that $m = 1 - \frac{1}{n}$. We explored the effect of relaxing this restriction in the fitting process but since there was little or no benefit in the quality of the fits obtained the restriction on m was kept.

3.3 Assumptions and limitations

In the present scheme, the pore structure is considered rigid, changes in aqueous phase saturation due to mineral reactions are disregarded, and the effect of variable liquid phase density on flow is neglected. All mineral phases in the system are assumed distributed uniformly throughout a computational cell, and are accessible to pore water regardless of the macroscopic moisture content. The residual moisture content is modelled as an immobile phase in flow and transport calculations but it is considered part of the soil solution in all geochemical reactions. This implies perfect mixing between the immobile and mobile pore water. Since the residual moisture content is not considered part of the water conducting pore space, the equivalent radius of water-filled pores is zero. It is expected that the tortuosity l in the conductivity-moisture relation is also affected by mineral reactions [80-82]. Nevertheless, l is left constant at the suggested value of 0.5 [66] in order to avoid invoking additional assumptions.

4 Influence of pore-size selectivity on hydraulic parameters

Using Eq. (19) the influence of mineral film development in the entire pore space versus pore-size selective mineral reactions (Eq. (13)) can be evaluated. Following the example of calcite precipitation in [29], a calcite supersaturated solution infiltrates into a soil column with fixed partial pressure of CO_2 at $10^{-1.5}$ atm. Kinetic calcite precipitation is simulated according to the rate equation [83]. Parameters, column properties, initial and boundary conditions of the simulation are summarized in Table 1.

Table 1 near here

Fig. 7a illustrates porosity, as θ_{sat} which corresponds directly to the volume change through precipitated calcite, together with saturated hydraulic conductivity (b) and the van Genuchten parameter α (c) after 7.5 h of continuous infiltration. In this simulation the influence of changed hydraulic properties on flow and solute transport is deactivated in order to evaluate the influence of pore-size selectivity with equal changes in mineral volume. In flow-coupled simulations the different alteration of hydraulic properties leads to different mineral precipitation patterns.

Fig. 7 near here

The results clearly show the large effect of pore-size selectivity on changes in saturated hydraulic conductivity. Compared to the case where the entire PSD is affected, the selective radius shift model predicts a considerably smaller reduction in saturated conductivity (80% non-selective versus 93% selective) with the same change in porosity. This difference is consistent with the consideration that the saturated conductivity is largely determined by the larger pores sizes. A small radius change in the larger pores therefore may affect conductivity more than a larger change in the small pore-size fraction.

5 Example application: Kinetic halite dissolution

In the following, the *selective radius shift* model is applied to investigate the effect of kinetic halite dissolution on the hydraulic properties of loamy sand [57].

The kinetics of halite dissolution is controlled by two distinct processes: NaCl detachment from the mineral surface according to surface coordination chemistry [84-87], and the transport of ions into the bulk solution through the interfacial layer quantified by transition state theory [88]. Alkattan et al. [89] proposed the overall reaction rate R (mol$T^{-1}M^{-1}$):

$$R = \left(\frac{k_c k_t}{k_c + k_t}\right) c_{eq,h}(1 - \Omega), \tag{26}$$

with saturation ratio Ω, equilibrium concentration of halite ions (Na, Cl) in solution $c_{eq,h}$, rate constants for the surface reaction effect k_c (T^{-1}) and rate constant for the transport effect k_t (T^{-1}). In the following simulations, the rate constants and equilibrium concentration k_c, k_t and $c_{eq,h}$ are combined into a single constant with the value of 0.2 mol (kg water)$^{-1}$ min^{-1}, which is within the range of experimentally determined reaction rates [89].

The rate at which ions are released/precipitated is strongly influenced by the mineral surface area in contact with the aqueous phase. However, the dependency of surface areas on mineral mass is dependent on the pore geometry. Parkhurst and Appelo [30], for instance, suggest a general reduction of surface area with decreasing mineral mass. This is in contradiction to the pore bundle concept, where the mineral surface increases with mineral dissolution. As noted by Steefel and Lasaga [15], “any number of methods can be used to calculate reactive surface areas, although none of them has been verified in a natural system”, thus here we choose to neglect the change of reactive surface area and its influence on the rate of halite reaction.

In the following, we present three simulations of a 50 cm long column with different initial and boundary conditions. The column has a cross sectional area of 10 dm^2 and contains loamy sand that is homogeneously amended with halite, which is the only non-inert mineral in the column. The initial pore water in the column is at equilibrium with the mineral phase and flushed with pure water. Simulation domain properties and initial hydraulic properties are summarized in Table 2.

Table 2 near here

5.1 Quasi steady state flow; high moisture content

The first simulation was carried out under moist conditions with boundary and initial conditions given as

$$t = 0, \quad z \geq 0, \quad \theta = 0.4, \quad c = c_{eq,h},$$
$$t \geq 0, \quad z = 0, \quad \theta = 0.4, \quad c = 0. \tag{27}$$

Fig. 8 illustrates the simulation results 60, 180 and 300 min after the start of pure water infiltration. The column profiles of Θ are shown in part (a). Small variations in Θ are mainly due to the increase of θ_{sat} in combination with a fixed moisture content boundary condition. Since the hydraulic properties within the medium change during the simulation, neither a constant flux nor a constant moisture content boundary leads to steady state flow conditions. A 20% increase in θ_{sat} is shown in part (b) of the graph. Since θ_{sat} is equivalent to the effective porosity, its increase reflects the volume of halite that has been removed from the pore space by kinetic dissolution. In the given moisture conditions the flow velocities are on the same timescale as the reaction kinetics, such that mineral volumes decline more gradually than the step change that is typical for equilibrium reactions. The van Genuchten parameters α and n generally increase, as shown in parts (c) and (d). In the first 5 cm of the column a decrease of α is observed, which is due to the initial perturbation of the flow, where dissolution proceeds at a slightly lower soil moisture content. The saturated hydraulic conductivity K_{sat} in part (e) almost doubles during the course of the simulation, driven by the increase in θ_{sat} and enhanced by the general increase in α.

Fig. 8 near here

The change in the van Genuchten shape parameter n indicates the increasing importance of larger pore sizes in the substrate. With increasing n, α, K_{sat} and θ_{sat} the medium evolves from a loamy sand towards sand, according to the categorization of soils in Leij et al. [57].

5.2 Quasi steady state flow; low moisture content

This simulation was performed with the same column properties (Table 2) but with different moisture conditions to the previous example in order to demonstrate the effect of saturation on hydraulic properties. Boundary and initial conditions were

$$t = 0, \quad z \geq 0, \quad \theta = 0.2, \quad c = c_{eq,h},$$
$$t \geq 0, \quad z = 0, \quad \theta = 0.2, \quad c = 0. \tag{28}$$

Fig. 9a shows again a small perturbation of the initial steady state moisture content, caused by the changes of hydraulic properties. Due to low water contents and long residence time in a computational cell, dissolution nearly reaches local thermodynamic equilibrium during a time step. The solution becomes saturated with respect to halite in the first cell that contains the mineral and no further dissolution takes place downstream. As a result, the increase in θ_{sat} in part (b) proceeds with a distinct step change. The large decrease in the van Genuchten parameters α and the almost constant n (parts (c) and (d)) results from the size selectivity of the dissolution reaction, which now only takes place in the fraction of the pore space that corresponds to small pore radii. Due to the decrease in α the increase in K_{sat} (part (e)) is reduced compared to the simulation at higher moisture contents.

Fig. 9 near here

6 Example application: Calcite precipitation due to cation exchange

This example illustrates the application of the *selective radius shift* model to the case of mineral precipitation occurring due to cation exchange during transient infiltration. The example is motivated by the frequently observed permeability reduction in reactive barriers, where minerals precipitate due to adsorption-desorption processes [43,44,90]. Reactive barriers are designed to protect groundwater aquifers from contamination by adsorbing pollutants (e.g., heavy metals) onto the solid soil structure. Therefore, materials with high cation exchange capacity are of particular interest in this remediation technique. The simulation is carried out for a clay loam with initially uniform hydraulic properties, which contains a potent exchanger at a depth of 10 cm downwards. Its cation exchange capacity is set to values that are extremely high for natural soils but can be reached by synthetic exchange materials [91] or organic adsorbents [92].

Initially the exchange sites are filled with calcium ions. The infiltrating solution contains a high ionic strength sodium carbonate solution at the saturation limit of natron. As soon as the infiltration front arrives at the exchange layer, calcium is replaced by sodium leading to a snowplough phenomenon [93-95], where concentrations of desorbed calcium exceed initial concentrations. In addition, the solution is allowed to equilibrate with respect to calcite, which immediately precipitates most of the released calcium ions due to high carbonate concentrations. The simulation properties are summarised in Table 3.

Table 3 near here

Reaction equations for cation exchange and calcite dissolution/precipitation are:

$$\begin{aligned} &2\mathrm{Na}^{+} + \mathrm{CaX}_2 = 2\mathrm{NaX} + \mathrm{Ca}^{+2} && \log(\mathcal{K}) = -0.80 \\ &\mathrm{CaCO}_3^{s} = \mathrm{CO}_3^{-2} + \mathrm{Ca}^{+2} && \log(\mathcal{K}) = -8.48 \end{aligned} \tag{29}$$

Initial and boundary conditions are:

$$\begin{aligned} &t = 0, && z \geq 0, && \theta = 0.1, && c = 0, \\ &t \geq 0, && z = 0, && \theta = 0.3, && c = c_{eq,n}, \end{aligned} \tag{30}$$

where $c_{eq,n}$ denotes equilibrium concentration of sodium carbonate with natron.

Results of geochemical parameters are illustrated as column profiles in Fig. 10. Part (a) shows the development of molal sodium concentrations. In the first profile after 5 d, the infiltrating sodium has reached the reactive barrier and starts to replace calcium ions from the exchange. At later times the progress of sodium concentrations is strongly retarded compared to the moisture front due to continuous uptake by the exchanger. Part (b) shows the molal calcium concentrations in solution. Due to the precipitation of calcite, calcium concentrations in solution are low (< 0.2 millimolal) despite the large amounts that are replacement from the exchanger (2 mol (l soil)$^{-1}$). Parts (c) and (d) show amounts of adsorbed calcium and sodium, respectively. Because of the large abundance of sodium ions, calcium is almost completely removed from the exchanger despite preferential adsorption of calcium over sodium. Part (e) shows the total amount of precipitated calcite. Owing to high carbonate concentrations the moles of precipitated calcite are almost equal to the moles of initially adsorbed calcium.

Fig. 10 near here

Changes in hydraulic properties that result from calcite precipitation are displayed in Fig. 11. Part (a) illustrates the moisture profiles that results from infiltration into the initially dry medium with a constant moisture content boundary. The first snapshot after 5 d shows an undisturbed infiltration profile in a homogenous clay loam. In subsequent profiles, the moisture content shows small perturbations that result from space and time dependent hydraulic properties. In regions where calcite has precipitated the moisture content is generally lower, mainly due to reduced effective porosity. Part (b) shows the reduction in effective porosity that immediately follows from calcite precipitation. Profiles of the van Genuchten characteristic curve parameters α and n, displayed in parts (c) and (d) of the figure, show that n is more sensitive to the moisture content and therefore pore-size selectivity of the reaction than α under the simulated conditions. The increase in n indicates a decreasing contribution of small pore sizes to the total pore volume. Despite the increase in α a general reduction of K_{sat} is observed in part (e). However, the increase in α with precipitation at higher moisture contents can be traced in slightly smaller decreases of K_{sat}.

Fig. 11 near here

The development of the PSD of the clay loam is displayed in Fig. 12. In contrast to the loamy sand in the previous example, clay loam shows a monotone decrease of $f(r)$ with increasing pore radius. In terms of the van Genuchten formula, this monotone behaviour occurs for $n > 2$. In addition, the size selectivity with preferential decrease of small pore sizes as a result of precipitation in unsaturated conditions is displayed. Comparison of the PSD's at 10 and 16 cm shows a larger decrease of pore sizes between 2×10^{-4} and 3×10^{-3} cm during precipitation at larger soil moisture (16 cm) than during precipitation at lower soil moisture (10 cm). However, a magnification of the final PSD's at radii from 1.1×10^{-4} to 1.14×10^{-4} (insert Fig. 12) reveals a crossover of the PSD's after precipitation, which verifies more precipitation in smaller pores at lower moisture contents.

Fig. 12 near here

The influence of pore-size selective mineral reactions on the conductivity-moisture relations (Eq. (16)) is presented in Fig. 13. Although at first sight counterintuitive, we observe a hydraulic conductivity increase with mineral precipitation at a given θ. This is partially due to the increase of Θ with decreasing θ_{sat}. However, by plotting K in terms of Θ the influence of θ_{sat} on hydraulic conductivity is eliminated. The hydraulic conductivity-moisture content curves in Fig. 13 are therefore only dependent on K_{sat} and n. The fact that the conductivity-moisture relation after mineral reaction at 10 cm depth is still above the original curve at given Θ results from pore-size selectivity precipitation and hence change in n. As mentioned already, larger values of n are associated with a lower contribution of small pores to the total pore volume. Thus, at same Θ, a higher proportion of water is carried through large pores in the medium with precipitated calcite. The effect of reduced K_{sat} dominates the change in n only in moist conditions with Θ above 0.92 (insert in Fig. 13).

Fig. 13 near here

7 Discussion

7.1 Discussion of modelling results

From the example simulations, it can be seen that mineral reactions can have an important impact on the soil moisture characteristic and hydraulic conductivity-moisture content relationship.

Comparing the simulations in §5.1 and §5.2, the influence of the degree of saturation on the final retention parameters and saturated conductivity becomes obvious. The different evolution of α, with a small increase at a high moisture content and a strong decrease at a low moisture content has a marked influence on K_{sat} according to Eq. (18): K_{sat} increases by about 73% at for the high moisture content case compared to about 32% for the low moisture content case, despite the same increase in porosity for each case. This occurs because a medium with a high proportion of small pores exhibits a larger resistance to flow than a medium with large pores amounting to the same pore volume. Nevertheless, most models for hydraulic properties changes neglect the influence of the PSD on permeability, even though its influence is considerable in calculations of flow and transport even in fully saturated situations where flow is governed by K_{sat} alone.

The case of calcite precipitation (§6) demonstrates the capability of the new simulation tool to integrate complex geochemical reactions such as adsorption and desorption processes. Although this simple example is not a realistic representation of geochemical processes in a reactive barrier, the potential key mechanism for exchange-induced permeability reduction is captured. In the region of the exchanger, moisture contents increase gradually from relatively dry ($\theta = 0.1$) to moist conditions ($\theta = 0.3$), which highlights the influence of soil moisture on the change in soil moisture characteristics and hydraulic conductivity. In the first few centimetres of the exchanger layer, precipitation takes place in the tip of the diffuse moisture front at low moisture contents. As a result of the exchange process, the precipitation front becomes increasingly retarded with respect to the moisture front so that precipitation takes place at higher soil moisture within the reactive barrier. The resulting PSD's in Fig. 12 verify the conceptualization of saturation-dependent, pore-size selective mineral reactions with a larger reduction of smaller pore sizes in dry conditions. Increasing final values of α and decreasing n in the exchange layer represent the change in moisture content at which the mineral reaction takes place.

Interestingly, the reduction in permeability is largest close to the upper boundary of the exchanger layer, where it reduces the infiltration capacity at full saturation (K_{sat}). However, it is important to note that the actual value of unsaturated conductivity is not only dependent on K_{sat} but also on n, θ_{sat} and last but not least θ. Thus, the unsaturated conductivity cannot be inferred from hydraulic parameters alone but is directly interrelated with flow.

7.2 General model discussion

A principle criticism of any 1D simulation of mineral reactions and flow is the fact that self-enhancing instability phenomena cannot be captured. Within the domain of reactive flow in unsaturated soils three main types of interfering instabilities occur: (i) reaction instabilities due to initial heterogeneities in the hydraulic properties with dissolution of wormholes and karst phenomena [1,96-105], (ii) flow instabilities with moisture content fingering during the infiltration of a moisture front [106-116] and (iii) density instabilities due to local differences of solution densities [117-124]. However, the scope of this paper is not to investigate instability phenomena, but to propose a new approach that relates changes in mineral volumes and hydraulic properties. The validity of the current 1D model is therefore restricted to regions along flow lines with lateral homogeneity. With an integration of the proposed model for pore-size selective mineral reactions into a 3D reactive flow and transport simulator, interactions and feedbacks between instability phenomena could be investigated. Conceptually speaking, the approach presented here could be included in a 3D model, but at the cost of the loss of the tight coupling with PHREEQC achieved in the present 1D model. This tight coupling gives a significant benefit in that the full suite of PHREEQC's geochemical modelling capabilities is available.

The bundle of capillary tubes model, which is the foundation of the presented model, has been critically reviewed by Larson et al. [26], who stated three major inadequacies:

- The use of $\cos\phi$ in Eq. (2) as a measure of wettability does not adequately describe real porous media.
- The irregular geometry of real porous matrices and associated effects (e.g., inkbottle effect) are ignored.
- The connectivity and "branchiness" of real porous media is ignored.

Lehmann et al. [125] therefore conclude that the PSD's derived from the capillary pressure/fluid saturation relationship does not correspond to the geometrical PSD. Despite these shortcomings, the capillary tube model is widely applied as a simple link between continuum-scale hydraulic properties and PSD's [17,18,29,126]. The concept of modifying pore volumes through mineral reactions can be integrated also into more sophisticated pore network models that can be used to relate PSD's to soil moisture characteristic curves.

Our main contribution here is the advancement of existing models for the effect of chemical reactions on physical transport properties in unsaturated soils. As mentioned in §2.4, our model draws upon the Taylor model for biofilm growth [18]. When that model is applied to bioclogging, L_{fT} in Eq. (22) is restricted to negative values, which gives physically plausible results. However, the same model was applied to mineral reactions in the vadose zone for precipitation, $L_{fT} < 0$, and for dissolution, $L_{fT} > 0$ [29]. Starting from either the van Genuchten or the Books and Corey models [127], the pore number distribution, $P(r) = \frac{f(r)}{r^2}$, that results from the pore bundle concept has a singularity at zero radius. Thus, any additive increase in pore radii due to dissolution leads to infinite pore volume and permeability. Freedman et al. [29] only arrived at meaningful results by discretising the radius spectrum and therefore neglecting small pore sizes before applying radius changes due to mineral dissolution.

In our model, the approach of Taylor et al. [18] is adapted such that the volume change in each pore is proportional to its current volume (Eq. (10)). This proportionality assumes a strict dependency of mineral reactions on local solution concentrations. As this dependency is a macroscopic characteristic of the system, different pore scale behaviours could be envisaged, e.g., pore-size dependent nucleation site density. The application of any film-type model to mineral reactions relies on the assumption that precipitation and dissolution occurs homogeneously along pore walls (thin film assumption). Thus, the model is not applicable to the precipitation of large crystal-forming minerals. The joining of pores due to dissolution reactions and the resulting changes in PSD's and hydraulic properties is neglected. Together with the assumption of a rigid pore structure the model is therefore only valid for a limited amount of mineral dissolution.

Clement et al. [17] recognize the functional dependency of the saturated conductivity on α for the combination of the van Genuchten model with the Mualem conductivity. For cylindrical pores with effective lengths proportional to radii they arrive at a simple relation between permeability and changes in porosity according to

$$\frac{K_{sat}^*}{K_{sat}} = \left(\frac{\theta_{sat}^*}{\theta_{sat}}\right)^{\frac{19}{6}}. \tag{31}$$

However, since their model assumes that there is a proportionality between changes in maximum pore radius and porosity the model is not applicable to unsaturated conditions where the large pore sizes are unaffected by dissolution/precipitation reactions. In general, power laws that are based on an analogy to unsaturated conductivity only apply if changes in porosity affect the largest pores in the PSD. Reactions in unsaturated soils, however, affect only the small pore-size fraction, making application of a power law unsuitable. Here, we fit a single water retention curve that equally represents the reaction-affected and inert part of the pore space, and so obtain a new α that can be used directly to calculate changes in K_{sat}.

Taylor et al. [128] apply a statistic approach to relate dispersivities in pristine and bioclogging-affected soils. However, in a porous medium whose PSD is derived from a van Genuchten retention function the described procedure is inapplicable since the conductance distribution function exhibits a singularity at zero conductance and thus the variance of conductance is not well-defined. The combined simulation of flow solute transport, reactions and changes in hydraulic properties is therefore limited to situations were changes in dispersivities do not significantly affect reaction patters e.g., through the dominance of advective transport.

8 Conclusions

In this study, a new model for the effect of mineral dissolution/precipitation on hydraulic properties of unsaturated soils is developed and applied to the case of kinetic halite dissolution in loamy sand and equilibrium calcite precipitation due to cation exchange in clay loam. In contrast to existing approaches, the model divides the pore spectrum in an inert, dry part and a reaction-affected wet part, whose pore-size distribution (PSD) is changed according to changes in mineral volumes. Pore radii in the reactive part are modified such that the change in pore volume over a time step in the discretised numerical model is proportional to the pore volume itself. Combining the inert and reaction-affected PSD’s results in a piecewise retention curve, to which a new continuous soil moisture characteristic function is fitted in order to smooth unphysical discontinuities and obtain a single set of retention parameters. The updated retention parameters are directly used to calculate changes in saturated hydraulic conductivity.

The model is integrated into a numerical scheme for comprehensive geochemical reactions and unsaturated solute transport where, because reactions vary in time and space, each cell in the discretised model domain has time-dependent hydraulic properties characterized by a single set of hydraulic parameters. Because of the sensitivity of results on the fitting procedure and accumulating fitting errors, a penalty function is introduced into the objective function of the downhill simplex method in order to avoid unphysical results.

The examples give further insight into the effect of moisture content on the spatial and temporal evolution of PSD’s and retention parameters θ_{sat}, n and α. The evolution of porous media is demonstrated for the case of kinetic mineral dissolution and precipitation due to cation exchange in a simplified reactive barrier.

The main finding of the simulations is the strong influence of the degree of saturation on changes in K_{sat}, which could not be determined without considering an unsaturated flow model. In the example given (§4), equal changes in porosity lead to increases in K_{sat} of about 73% at high moisture content compared to 32% at low moisture content. The difference is due to the relative importance of small pore sizes, as reflected in the quadratic influence of the van Genuchten parameter α on K_{sat}, which accounts for the. The same general tendency is found in simulations of transient infiltration. Especially under condition of low saturation, permeability models that rely on porosity alone [e.g., 17,22,63,129] greatly misestimate K_{sat} for changes in porosity in unsaturated conditions.

Although at first sight counterintuitive, for unsaturated conditions the moisture content-dependent hydraulic conductivity, $K(\theta)$ increases due to mineral precipitation and decreases during dissolution at given θ. This is mostly due to the dependency of the Mualem conductivity on Θ and changes in θ_{sat}. However, from Fig. 13 it can be concluded that even at same reduced moisture content, the unsaturated hydraulic conductivity changes in the opposite direction to θ_{sat} and K_{sat} over most of the moisture spectrum if mineral reactions take place at low moisture contents. This result becomes obvious considering that after precipitation in small pores water has to be carried through larger pores that pose less resistance to flow and vice versa for dissolution.

The model offers the potential for experimental confirmation of the development of PSD's by measurements before and after mineral reaction reactions.

Acknowledgments

This research is supported by Alcoa World Alumina Australia.

References

[1] Lichtner PC. Continuum formulation of multicomponent-multiphase reactive transport. In Lichtner PC, Steefel CI, and Oelkers EH, editors. Reactive transport in porous media. Washington DC: Mineralogical Society of America; 1996. p. 82-129.

[2] Lichtner PC. FLOTRAN user manual. Los Alamos National Laboratory LA-UR-01-2349, 2000.

[3] Mayer KU. A numerical model for multicomponent reactive transport in variably saturated porous media Ph.D. thesis, University of Waterloo, 1999.

[4] Xu T, Sonnenthal EL, Spycher N, and Pruess K. TOUGHREACT user's guide: A simulation program for non-isothermal multiphase reactive geochemical transport in variably saturated geologic media. Lawrence Berkeley National Laboratory LBNL-55460, 2004.

[5] Jacques D and Šimůnek J. User manual of the multicomponent variably- saturated flow and transport model HP1. SCK•CEN Waste & Disposal Department 2005.

[6] Lichtner PC. Continuum model for simultaneous chemical-reactions and mass-transport in hydrothermal systems. *Geochim Cosmochim Ac* 1985;49(3):779-800.

[7] Hassanizadeh SM. Derivation of basic equations of mass-transport in porous-media. 2. Generalized Darcy and Fick laws. *Adv Water Resour* 1986;9(4):207-22.

[8] Bear J and Verruijt A. Modeling groundwater flow and pollution. Dordrecht: D. Reidel, 1987.

[9] Barry DA. Supercomputers and their use in modeling subsurface solute transport. *Rev Geophys* 1990;28(3):277-95.

[10] Li L, Peters CA, and Celia MA. Upscaling geochemical reaction rates using pore-scale network modeling. *Adv Water Resour* 2006;29(9):1351-70.

[11] Meile C and Tuncay K. Scale dependence of reaction rates in porous media. *Adv Water Resour* 2006;29(1):62-71.

[12] Lichtner PC and Kang Q. Upscaling pore-scale reactive transport equations using a multiscale continuum formulation. *Water Resour Res* 2007;43(12)

[13] Hassanizadeh SM. Derivation of basic equations of mass-transport in porous-media. 1. Macroscopic balance laws. *Adv Water Resour* 1986;9(4):196-206.

[14] Panda MN and Lake LW. A physical model of cementation and its effects on single-phase permeability. *AAPG (Am Assoc Pet Geol) Bull* 1995;79(3):431-43.

[15] Steefel CI and Lasaga AC. A coupled model for transport of multiple chemical-species and kinetic precipitation dissolution reactions with application to reactive flow in single-phase hydrothermal systems. *Am J Sci* 1994;294(5):529-92.

[16] Baveye P and Valocchi A. An evaluation of mathematical-models of the transport of biologically reacting solutes in saturated soils and aquifers. *Water Resour Res* 1989;25(6):1413-21.

[17] Clement TP, Hooker BS, and Skeen RS. Macroscopic models for predicting changes in saturated porous media properties caused by microbial growth. *Ground Water* 1996;34(5):934-42.

[18] Taylor SW, Milly PCD, and Jaffé PR. Biofilm growth and the related changes in the physical-properties of a porous-medium. 2. Permeability. *Water Resour Res* 1990;26(9):2161-69.

[19] Cochepin B, Trotignon L, Bildstein O, Steefel CI, Lagneau V, and Der Lee JV. Approaches to modeling coupled flow and reaction in a 2-D cementation experiment. *Adv Water Resour*:In Press, Accepted Manuscript.

[20] Purcell WR. Capillary pressures - their measurement using mercury and the calculation of permeability therefrom. *T Am I Min Met Eng* 1949;186(2):39-48.

[21] Miller EE and Miller RD. Physical theory for capillary flow phenomena. *J Appl Phys* 1956;27(4):324-32.

[22] Scheidegger AE. The physics of flow through porous media. Toronto: University of Toronto Press, 1974.

[23] Blake FC. The resistance of packing to fluid flow. *T Am I Chem Eng* 1921;14:415-21.

[24] Fatt I. The network model of porous media. 1. Capillary pressure characteristics. *T Am I Min Met Eng* 1956;207(7):144-59.

[25] Fatt I. The network model of porous media. 2. Dynamic properties of a single size tube network. *T Am I Min Met Eng* 1956;207(7):160-63.

[26] Fatt I. The network model of porous media .3. Dynamic properties of networks with tube radius distribution. *T Am I Min Met Eng* 1956;207(7):164-81.

[27] Larson RG, Scriven LE, and Davis HT. Percolation theory of 2 phase flow in porous-media. *Chem Eng Sci* 1981;36(1):57-73.

[28] Saripalli KP, Meyer PD, Bacon DH, and Freedman VL. Changes in hydrologic properties of aquifer media due to chemical reactions: A review. *Crit Rev Environ Sci Technol* 2001;31(4):311-49.

[29] Freedman VL, Bacon DH, Saripalli KP, and Meyer PD. A film depositional model of permeability for mineral reactions in unsaturated media. *Vadose Zone J* 2004;3(4):1414-24.

[30] Parkhurst DL and Appelo CAJ. User's guide to PHREEQC (version 2): A computer program for speciation, batch-reaction, one-dimensional transport, and inverse geochemical calculations. USGS 1999.

[31] Milopoulos PG, Suidan MT, Sayles GD, and Kaskassian S. Numerical modeling of oxygen exclusion experiments of anaerobic bioventing. *J Contam Hydro* 2002;58(3-4):209-20.

[32] Livingston RJ and Islam MR. Laboratory modeling, field study, and numerical simulation of bioremediation of petroleum contaminants. *Energ Source* 1999;21(1-2):113-29.

[33] Cortes-Jimenez JM, Troyo-Dieguez E, Murillo-Amador B, Garcia-Hernandez JL, Garatuza-Payan J, and Lee SS. Diagnosing and modeling water quality parameters of the Yaqui valley's aquifer in northwest Mexico for salinity risk evaluation. *Fresen Environ Bull* 2007;16(5):517-23.

[34] Xu P and Shao YP. A salt-transport model within a land-surface scheme for studies of salinisation in irrigated areas. *Environ Modell Softw* 2002;17(1):39-49.

[35] Kroes JG, Wesseling JC, and Van Dam JC. Integrated modelling of the soil-water-atmosphere-plant system using the model SWAP 2.0. An overview of theory and an application. *Hydrol Process* 2000;14(11-12):1993-2002.

[36] Ali R, Elliott RL, Ayars JE, and Stevens EW. Soil salinity modeling over shallow water tables. 1. Validation of LEACHC. *J Irrig Grain E-ASCE* 2000;126(4):223-33.

[37] Ducloux J, Guero Y, Fallavier P, and Valet S. Mineralogy of salt efflorescences in paddy field soils of Kollo, Southern Niger. *Geoderma* 1994;64(1-2):57-71.

[38] Mees F and Stoops G. Mineralogical study of salt efflorescences on soils of the Jequetepeque Valley, Northern Peru. *Geoderma* 1991;49(3-4):255-72.

[39] Nassar IN and Horton R. Salinity and compaction effects on soil water evaporation and water and solute distributions. *Soil Sci Soc Am J* 1999;63(4):752-58.

[40] Wantanaphong J, Mooney SJ, and Bailey EH. Quantification of pore clogging characteristics in potential permeable reactive barrier (PRB) substrates using image analysis. *J Contam Hydro* 2006;86(3-4):299-320.

[41] Henderson AD and Demond AH. Long-term performance of zero-valent iron permeable reactive barriers: A critical review. *Environ Eng Sci* 2007;24(4):401-23.

[42] Van Nooten T, Lieben F, Dries J, Pirard E, Springael D, and Bastiaens L. Impact of microbial activities on the mineralogy and performance of column-scale permeable reactive iron barriers operated under two different redox conditions. *Environ Sci Technol* 2007;41(16):5724-30.

[43] Parbs A, Ebert M, and Dahmke A. Influence of mineral precipitation on the performance and long-term stability of Fe-0-permeable reactive barriers: A review on the basis of 19 Fe-0-reactive barrier sites. *Grundwasser* 2007;12(4):267-81.

[44] Li L, Benson CH, and Lawson EM. Modeling porosity reductions caused by mineral fouling in continuous-wall permeable reactive barriers. *J Contam Hydro* 2006;83(1-2):89-121.

[45] Jiricek M, Sracek O, and Janda V. Removal of chlorinated solvents from carbonate-buffered water by zero-valent iron. *Cent Eur J Chem* 2007;5(1):87-106.

[46] Mayer KU, Blowes DW, and Frind EO. Reactive transport modeling of an in situ reactive barrier for the treatment of hexavalent chromium and trichloroethylene in groundwater. *Water Resour Res* 2001;37(12):3091-103.

[47] Celia MA, Bouloutas ET, and Zarba RL. A general mass-conservative numerical-solution for the unsaturated flow equation. *Water Resour Res* 1990;26(7):1483-96.

[48] Gupta AD, Lake LW, Pope GA, Sepehrnoori K, and King MJ. High-resolution monotonic schemes for reservoir fluid-flow simulation. *In Situ* 1991;15(3):289-317.

[49] Steefel CI and Lasaga AC. A coupled model for transport of multiple chemical species and kinetic precipitation dissolution reactions with application to reactive flow in single-phase hydrothermal systems. *American Journal of Science* 1994;294(5):529-92.

[50] Wissmeier L and Barry DA. Reactive transport in unsaturated soil: Comprehensive modelling of the dynamic spatial and temporal mass balance of water and chemical components. *Adv Water Resour* 2008;31(5):858-75.

[51] Washburn EW. Note on a method of determining the distribution of pore sizes in a porous material. *P Natl Acad Sci USA* 1921;7:115-16.

[52] Haverkamp R and Parlange JY. Predicting the water-retention curve from particle-size distribution. 1. Sandy soils without organic-matter. *Soil Sci* 1986;142(6):325-39.

[53] Hammecker C, Barbiero L, Boivin P, Maeght JL, and Diaw EHB. A geometrical pore model for estimating the microscopical pore geometry of soil with infiltration measurements. *Transport Porous Med* 2003;54(2):193-219.

[54] Wise WR, Clement TP, and Molz FJ. Variably saturated modeling of transient drainage: Sensitivity to soil properties. *J Hydro* 1994;161(1-4):91-108.

[55] van Genuchten MT. Closed-form equation for predicting the hydraulic conductivity of unsaturated soils. *Soil Sci Soc Am J* 1980;44(5):892-98.

[56] Wolfram MathWorld. Heaviside step function. http://mathworld.wolfram.com/HeavisideStepFunction.html, Date of Access: 14.07.2008.

[57] Leij FJ, Russell WB, and Lesch SM. Closed-form expressions for water retention and conductivity data. *Ground Water* 1997;35(5):848-58.

[58] Millington RJ and Quirk JP. Permeability of porous media. *Nature* 1959;183(4658):387-88.

[59] Hazen A. Some physical properties of sands and gravels, with special reference to their use in filtration, 24th annual report. Massachusetts State Board of Health 34, 1892.

[60] Marshall TJ. A relation between permeability and size distribution of pores. *J Soil Sci* 1958;9(1):1-8.

[61] Kozeny J. Über kapillare Leitung des Wassers im Boden - Aufstieg, Versickerung und Anwendung auf die Bewässerung. 1927.

[62] Fredlund DG, Xing AQ, and Huang SY. Predicting the permeability function for unsaturated soils using the soil-water characteristic curve. *Can Geotech J* 1994;31(4):533-46.

[63] Steefel CI. Geochemical kinetics and transport. In Brantley SL, Kubicki JD, and White AF, editors. Kinetics of water-rock interaction. New York: Springer; 2007. p. 545-89.

[64] Burdine NT. Relative permeability calculations from pore size distribution data. *T Am I Min Met Eng* 1953;198:71-78.

[65] Brovelli A, Malaguerra F, and Barry DA. Bioclogging in porous media: Model development and sensitivity to initial conditions. *Environ Modell Softw* 2009;24(5):611-26.

[66] Mualem Y. New model for predicting hydraulic conductivity of unsaturated porous-media. *Water Resour Res* 1976;12(3):513-22.

[67] van Genuchten MT and Nielsen DR. On describing and predicting the hydraulic-properties of unsaturated soils. *Ann Geophys* 1985;3(5):615-27.

[68] Maple 12; Maplesoft, a division of Waterloo Maple Inc. 2008

[69] Barry DA, Bajracharya K, and Miller CT. Alternative split-operator approach for solving chemical reaction groundwater transport models. *Adv Water Resour* 1996;19(5):261-75.

[70] Simpson MJ and Landman KA. Analysis of split operator methods applied to reactive transport with Monod kinetics. *Adv Water Resour* 2007;30(9):2026-33.

[71] Simpson MJ and Landman KA. Theoretical analysis and physical interpretation of temporal truncation errors in operator split algorithms. *Math Comput Simulat* 2008;77(1):9-21.

[72] Barry DA, Miller CT, Culligan PJ, and Bajracharya K. Analysis of split operator methods for nonlinear and multispecies groundwater chemical transport models. *Math Comput Simulat* 1997;43(3-6):331-41.

[73] Barry DA, Bajracharya K, Crapper M, Prommer H, and Cunningham CJ. Comparison of split-operator methods for solving coupled chemical non-equilibrium reaction/groundwater transport models. *Math Comput Simulat* 2000;53(1-2):113-27.

[74] Kanney JF, Miller CT, and Barry DA. Comparison of fully coupled approaches for approximating nonlinear transport and reaction problems. *Adv Water Resour* 2003;26(4):353-72.

[75] Jacques D, Šimůnek J, Mallants D, and van Genuchten MT. Operator-splitting errors in coupled reactive transport codes for transient variably saturated flow and contaminant transport in layered soil profiles. *J Contam Hydro* 2006;88(3-4):197-218.

[76] Barry DA, Prommer H, Miller CT, Engesgaard P, Brun A, and Zheng C. Modelling the fate of oxidisable organic contaminants in groundwater. *Adv Water Resour* 2002;25(8-12):945-83.

[77] Šimůnek J, van Genuchten MT, and Sejna M. The HYDRUS-1D software package for simulating the movement of water, heat, and multiple solutes in variably saturated

media, version 4.0. Department of Environmental Sciences, University of California Riverside 2008.

[78] Nelder JA and Mead R. A simplex-method for function minimization. *Comput J* 1965;7(4):308-13.

[79] Press WH, Teukolsky SA, Vetterling WT, and Flannery BP. Numerical recipes : The art of scientific computing. Cambridge: Cambridge University Press, 1990.

[80] Bradbury MH and Green A. Measurement of important parameters determining aqueous phase diffusion rates through crystalline rock matrices. *J Hydro* 1985;82(1-2):39-55.

[81] Bradbury MH and Stephen IG. Diffusion and permeability based sorption measurements in intact rock samples. in Materials Research Society Symposia Proceedings, 1986.

[82] Fujimaki H, Shimano T, Inoue M, and Nakane K. Effect of a salt crust on evaporation from a bare saline soil. *Vadose Zone J* 2006;5(4):1246-56.

[83] Plummer LN, Wigley TML, and Parkhurst DL. Kinetics of calcite dissolution in CO2-water systems at 5-degrees-C to 60-degrees-C and 0.0 to 1.0 atm CO2. *Am J Sci* 1978;278(2):179-216.

[84] Lichtner PC. The quasi-stationary state approximation to coupled mass-transport and fluid-rock interaction in a porous-medium. *Geochim Cosmochim Ac* 1988;52(1):143-65.

[85] Murphy WM, Oelkers EH, and Lichtner PC. Surface-reaction versus diffusion control of mineral dissolution and growth-rates in geochemical processes. *Chem Geol* 1989;78(3-4):357-80.

[86] Lichtner PC. Scaling properties of time-space kinetic mass-transport equations and the local equilibrium limit. *Am J Sci* 1993;293(4):257-96.

[87] Stumm W, Furrer G, and Kunz B. The role of surface coordination in precipitation and dissolution of mineral phases. *Croat Chem Acta* 1983;56(4):593-611.

[88] Lasaga AC. Rate laws in chemical reactions. In Lasaga AC and Kirkpatrick RJ, editors. Kinetics of geochemical processes. Washington, DC: Mineralogical Society of America; 1981. p. 135–69.

[89] Alkattan M, Oelkers EH, Dandurand J-L, and Schott J. Experimental studies of halite dissolution kinetics. 1. The effect of saturation state and the presence of trace metals. *Chem Geol* 1997;137(3-4):201-19.

[90] Mackenzie PD, Horney DP, and Sivavec TM. Mineral precipitation and porosity losses in granular iron columns. *J Hazard Mater* 1999;68(1-2):1-17.

[91] Kodama T, Gokon N, and Komarneni S. Novel synthetic clays for cation exchange. in 11th International Ceramics Congress: Advances in Science and Technology, 2006.

[92] Appelo CAJ and Postma D. Geochemistry, groundwater and pollution. Leiden: Balkema, 2005.

[93] Bajracharya K and Barry DA. Analysis of one-dimensional multispecies transport experiments in laboratory soil columns. *Environ Int* 1995;21(5):687-91.

[94] Appelo CAJ. Some calculations on multicomponent transport with cation-exchange in aquifers. *Ground Water* 1994;32(6):968-75.

[95] Barry DA, Starr JL, Parlange JY, and Braddock RD. Numerical-analysis of the snow-plow effect. *Soil Sci Soc Am J* 1983;47(5):862-68.

[96] Ortoleva P, Chadam J, Merino E, and Sen A. Geochemical self-organization. 2. The reactive-infiltration instability. *Am J Sci* 1987;287(10):1008-40.

[97] Ortoleva P, Merino E, Moore C, and Chadam J. Geochemical self-organization. 1. Reaction-transport feedbacks and modeling approach. *Am J Sci* 1987;287(10):979-1007.

[98] Sherwood JD. Stability of a plane reaction front in a porous-medium. *Chem Eng Sci* 1987;42(7):1823-29.

[99] Sherwood JD. Unstable fronts in a porous-medium. *J Comput Phys* 1987;68(2):485-500.

[100] Hinch EJ and Bhatt BS. Stability of an acid front moving through porous rock. *J Fluid Mech* 1990;212:279-88.

[101] Steefel CI and Lasaga AC. Evolution of dissolution patterns - permeability change due to coupled flow and reaction. in ACS Symposium Series, 1990.

[102] Groves CG and Howard AD. Early development of karst systems. 1. Preferential flow path enlargement under laminar-flow. *Water Resour Res* 1994;30(10):2837-46.

[103] Hanna RB and Rajaram H. Influence of aperture variability on dissolutional growth of fissures in karst formations. *Water Resour Res* 1998;34(11):2843-53.

[104] Clemens T, Huckinghaus D, Liedl R, and Sauter M. Simulation of the development of karst aquifers: Role of the epikarst. *Int J Earth Sci* 1999;88(1):157-62.

[105] Dahan O, Nativ R, Adar EM, Berkowitz B, and Weisbrod N. On fracture structure and preferential flow in unsaturated chalk. *Ground Water* 2000;38(3):444-51.

[106] Glass RJ, Cann S, King J, Baily N, Parlange JY, and Steenhuis TS. Wetting front instability in unsaturated porous-media: A 3-dimensional study in initially dry sand. *Transport Porous Med* 1990;5(3):247-68.

[107] Glass RJ, Parlange JY, and Steenhuis TS. Wetting front instability. 1. Theoretical discussion and dimensional analysis. *Water Resour Res* 1989;25(6):1187-94.

[108] Glass RJ, Steenhuis TS, and Parlange JY. Wetting front instability. 2. Experimental determination of relationships between system parameters and two-dimensional unstable flow field behavior in initially dry porous-media. *Water Resour Res* 1989;25(6):1195-207.

[109] Selker J, Leclerq P, Parlange JY, and Steenhuis T. Fingered flow in 2 dimensions. 1. Measurement of matric potential. *Water Resour Res* 1992;28(9):2513-21.

[110] Selker J, Parlange JY, and Steenhuis T. Fingered flow in 2 dimensions. 2. Predicting finger moisture profile. *Water Resour Res* 1992;28(9):2523-28.

[111] Selker JS, Steenhuis TS, and Parlange JY. Wetting front instability in homogeneous sandy soils under continuous infiltration. *Soil Sci Soc Am J* 1992;56(5):1346-50.

[112] Wang Z, Feyen J, and Elrick DE. Prediction of fingering in porous media. *Water Resour Res* 1998;34(9):2183-90.

[113] Hill DE and Parlange JY. Wetting front instability in layered soils. *Soil Sci Soc Am Pro* 1972;36(5):697-702.

[114] Parlange JY and Hill DE. Theoretical-analysis of wetting front instability in soils. *Soil Sci* 1976;122(4):236-39.

[115] Liu YP, Steenhuis TS, and Parlange JY. Closed-form solution for finger width in sandy soils at different water contents. *Water Resour Res* 1994;30(4):949-52.

[116] Parlange J-Y, Steenhuis TS, Li L, Barry DA, and Stagnitti F. Column flow in stratified soils and fingers in Hele-Shaw cells: A review. In Raats PAC, Smiles D, and Warrick AW, editors. Environmental mechanics: Water, mass and energy transfer in the biosphere. Washington, DC: American Geophysical Union; 2002. p. 79-85.

[117] Cooper CA, Glass RJ, and Tyler SW. Experimental investigation of the stability boundary for double-diffusive finger convection in a Hele-Shaw cell. *Water Resour Res* 1997;33(4):517-26.

[118] Cooper CA, Glass RJ, and Tyler SW. Effect of buoyancy ratio on the development of double-diffusive finger convection in a Hele-Shaw cell. *Water Resour Res* 2001;37(9):2323-32.

[119] Prasad A and Simmons CT. Unstable density-driven flow in heterogeneous porous media: A stochastic study of the Elder [1967b] "short heater'' problem. *Water Resour Res* 2003;39(1):1-21.

[120] Schincariol RA, Schwartz FW, and Mendoza CA. On the generation of instabilities in variable-density flow. *Water Resour Res* 1994;30(4):913-27.

[121] Schincariol RA, Schwartz FW, and Mendoza CA. Instabilities in variable density flows: Stability and sensitivity analyses for homogeneous and heterogeneous media. *Water Resour Res* 1997;33(1):31-41.

[122] Wooding RA, Tyler SW, and White I. Convection in groundwater below an evaporating salt lake. 1. Onset of instability. *Water Resour Res* 1997;33(6):1199-217.

[123] Brovelli A, Mao X, and Barry DA. Numerical modeling of tidal influence on density-dependent contaminant transport. *Water Resour Res* 2007;43(10)

[124] Mao X, Prommer H, Barry DA, Langevin CD, Panteleit B, and Li L. Three-dimensional model for multi-component reactive transport with variable density groundwater flow. *Environ Modell Softw* 2006;21(5):615-28.

[125] Lehmann P, Berchtold M, Ahrenholz B, Tölke J, Kaestner A, Krafczyk M, Flühler H, and Künsch HR. Impact of geometrical properties on permeability and fluid phase distribution in porous media. *Adv Water Resour* 2008:In Press, Corrected Proof.

[126] Hwang SI and Powers SE. Using particle-size distribution models to estimate soil hydraulic properties. *Soil Sci Soc Am J* 2003;67(4):1103-12.

[127] Brooks RH and Corey AT. Hydraulic properies of porous media. Civil Engineering Department, Colorado State University 1964.

[128] Taylor SW and Jaffe PR. Biofilm growth and the related changes in the physical-properties of a porous-medium .3. Dispersivity and model verification. *Water Resour Res* 1990;26(9):2171-80.

[129] Fair GM and Hatch LP. Fundamental factors governing the stream-line flow of water through sand. *J Am Wat Works Assoc* 1933;25:1551-65.

Figure captions

Fig. 1. Link between continuum-scale hydraulic properties and pore-size distribution via the pore bundle concept.

Fig. 2. Pore size distribution (a) and cumulative pore volume (b) of a porous medium undergoing selective mineral dissolution in the wet portion of the pore space. The overlap of wet and dry pore space that results from dissolution of wet pores with no redistribution of water during the reaction time step is marked by vertical lines.

Fig. 3. Soil moisture characteristic curves of the initial soil, after mineral dissolution according to Eq. (13) and the fitted van Genuchten moisture characteristic, Eq. (8).

Fig. 4. Development of the pore-size distribution according to the model by Taylor et al. [18] and the *selective radius shift model* with a reduction in effective porosity by 20.2 %.

Fig. 5. Sensitivity of saturated conductivity on changes in effective porosity according to the model of Taylor et al. [18] and the *selective radius shift model* in saturated moisture conditions.

Fig. 6. Flow chart of numerical model. Main computational modules are in bold, and variables that are passed between the modules are listed in the rounded boxes.

Fig. 7. Influence of pore-size selectivity on the development of hydraulic properties after 7.5 h of infiltration of a supersaturated calcite solution and kinetic calcite precipitation.

Fig. 8. Column profiles of main simulation results for kinetic halite dissolution at high water contents with infiltration of pure water at time 60, 180 and 300 min.

Fig. 9. Column profiles of main simulation results for kinetic halite dissolution at low water contents with infiltration of pure water at time 3000, 9000 and 15000 min.

Fig. 10. Column profiles of geochemical properties for calcite precipitation due to cation exchange with infiltration of sodium carbonate solution at time 5, 20, 200 and 450 d.

Fig. 11. Column profiles of moisture content and hydraulic properties for calcite precipitation due to cation exchange with infiltration of sodium carbonate solution at time 5, 20, 200 and 450 d.

Fig. 12. Effect of calcite precipitation on pore size distribution for time-varying moisture content at different locations in the exchange layer. Insert: Magnification of pore-size distribution at cross-over pore radius.

Fig. 13. Conductivity-moisture content relation of original clay loam (5 cm) and in the exchange layer after calcite precipitation. Insert: Magnification of conductivity relation close to full moisture saturation.

Tables

Table 1: Parameters, column properties, initial and boundary conditions for the comparison of pore size selective precipitation and precipitation in entire PSD.

Domain properties	
Column length	0.4 m
Cell length	0.01 m
Time step	450 s
Cross section area	0.1 m^2
Initial hydraulic properties	
θ_{sat}	0.5
θ_{res}	0.085
α	4.4 m^{-1}
n	2.2
l	0.5
K_{sat}	2.1714×10^{-3} m s^{-1}
Initial conditions	
Water content	0.2
Temperature	25 °C
Partial pressure CO$_2$	10$^{-1.5}$
Boundary condition z= 0 m	
θ	0.2
Temperature	25 °C
Partial pressure CO$_2$	10$^{-1.5}$
$\Omega_{calcite}$	1.8
Boundary condition z= 0.4 m	
θ	0.2
Temperature	25 °C
Partial pressure CO$_2$	10$^{-1.5}$

Table 2: Domain properties and initial hydraulic parameters for simulation of kinetic halite dissolution.

Domain properties	
Column length	50 cm
Cell length	1 cm
Time step	1 min
Cross section area	10 dm^2
Initial hydraulic properties	
θ_{sat}	0.41
θ_{res}	0.057
α	0.124 cm^{-1}
n	2.28
l	0.5
K_{sat}	0.243 cm min^{-1}

Table 3: Domain properties and initial hydraulic parameters for simulation of calcite precipitation due to cation exchange.

Domain properties	
Column length	20 cm
Cell length	0.5 cm
Time step	0.1 d
Cross section area	10 dm^2
Initial hydraulic properties	
θ_{sat}	0.41
θ_{res}	0.095
α	0.019 cm^{-1}
n	1.31
l	0.5
K_{sat}	0.26 cm h^{-1}
l	0.5
Inflowing solution (mol/kgw)	
Na^+	2.858
CO_3^{-2}	1.429
pH	7
CEC[a] ($z \geq 10$ cm)	4 eq (kg soil)$^{-1}$

[a] Cation exchange capacity; initially filled with calcium ions

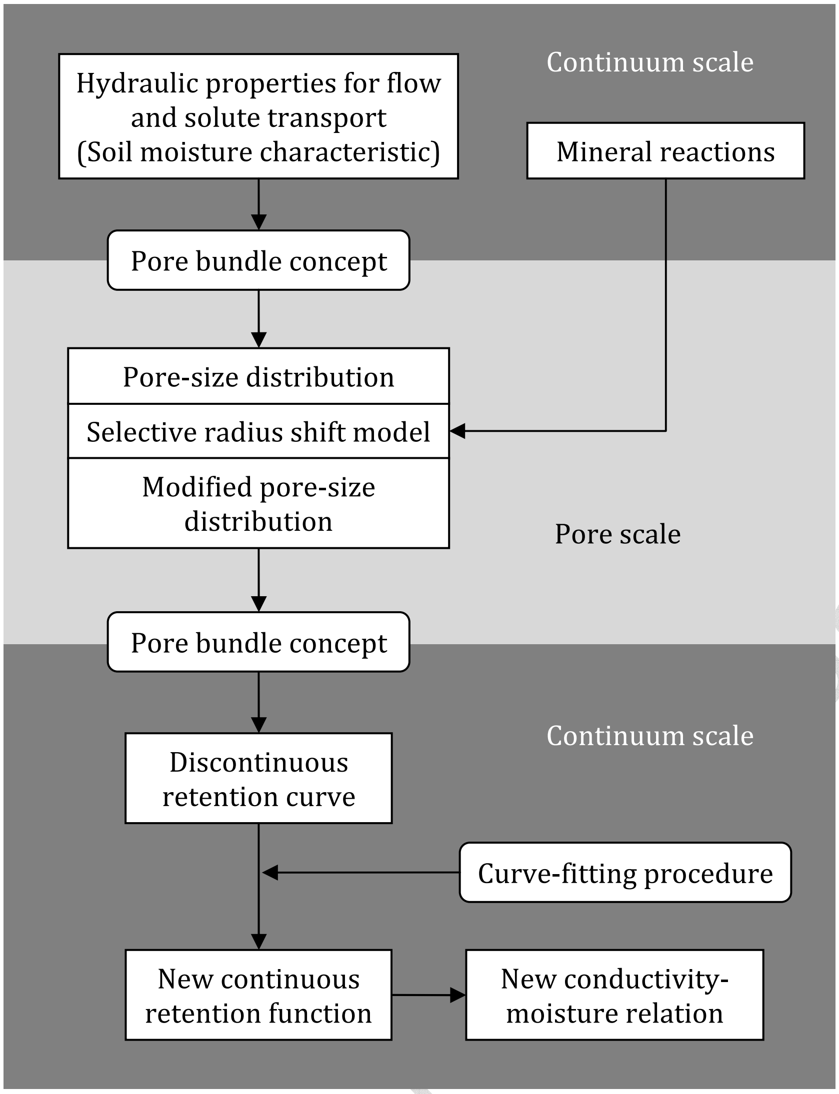
Continuum scale
Hydraulic properties for flow and solute transport (Soil moisture characteristic)
Mineral reactions
Pore bundle concept
Pore-size distribution
Selective radius shift model
Modified pore-size distribution
Pore scale
Pore bundle concept
Continuum scale
Discontinuous retention curve
Curve-fitting procedure
New continuous retention function
New conductivity-moisture relation

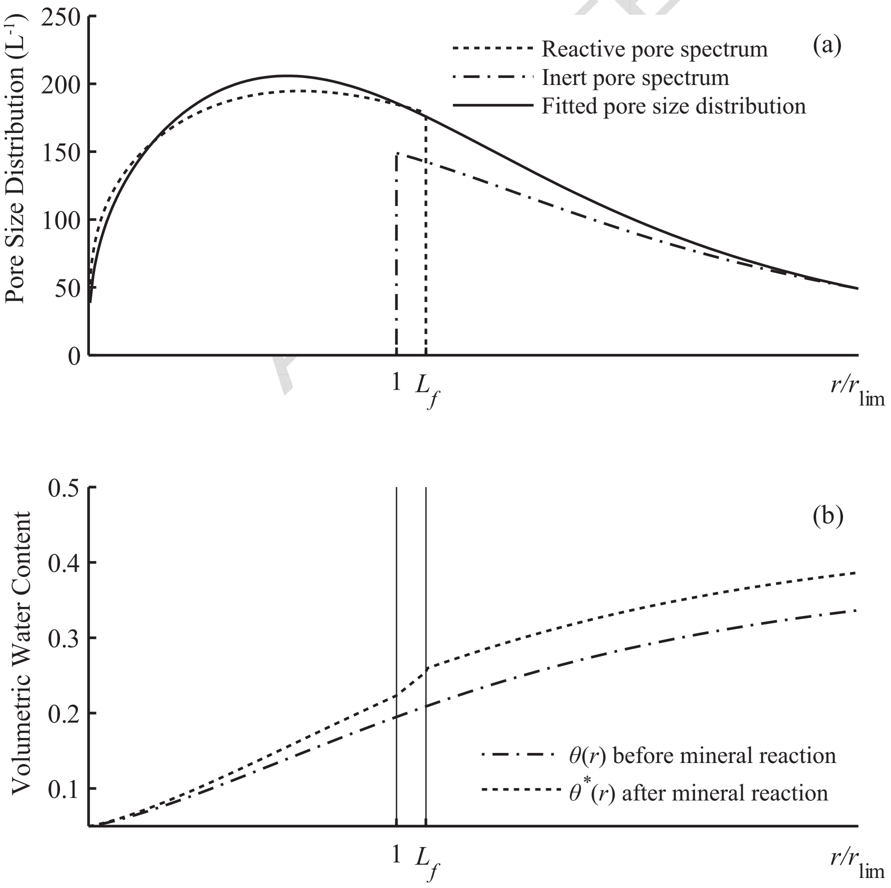
(a)
Pore Size Distribution (L^{-1})
250
200
150
100
50
0
Reactive pore spectrum
Inert pore spectrum
Fitted pore size distribution
1
L_f
$r/r_{\lim}$
(b)
Volumetric Water Content
0.5
0.4
0.3
0.2
0.1
$\theta(r)$ before mineral reaction
$\theta^*(r)$ after mineral reaction
1
L_f
$r/r_{\lim}$

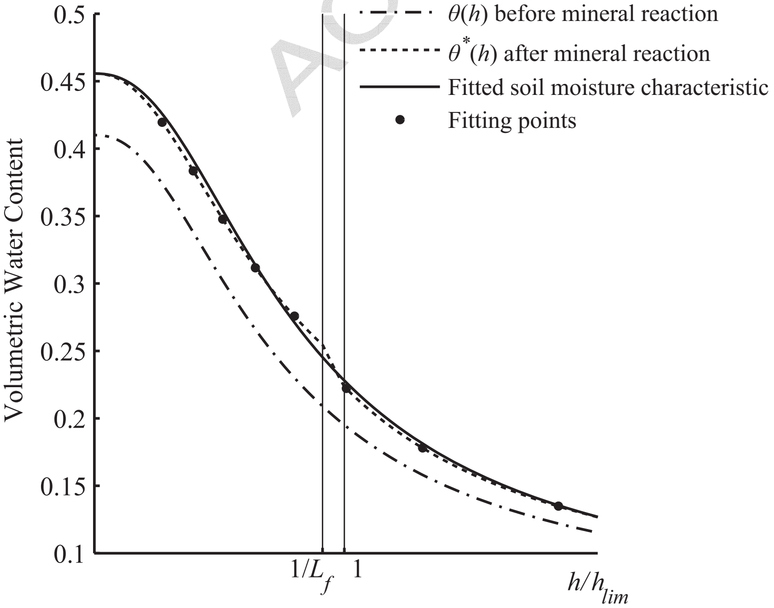

$\theta(h)$ before mineral reaction
$\theta^*(h)$ after mineral reaction
Fitted soil moisture characteristic
Fitting points
Volumetric Water Content
0.5
0.45
0.4
0.35
0.3
0.25
0.2
0.15
0.1
$1/L_f$
1
h/h_{lim}

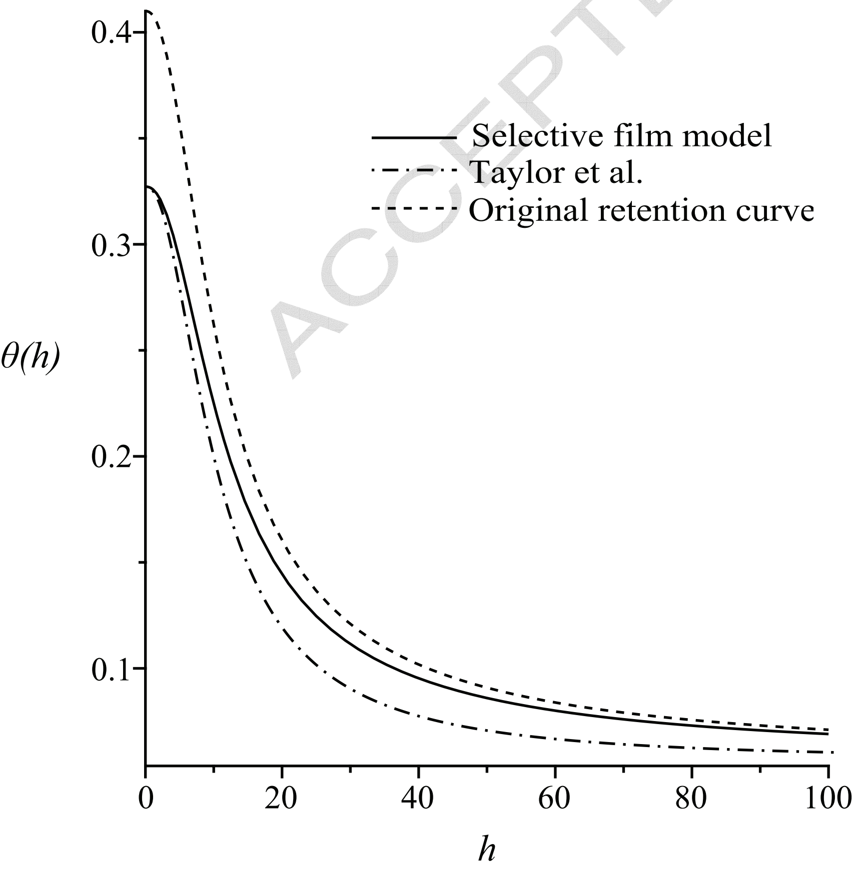
0.4
0.3
0.2
0.1
θ(h)
0
20
40
60
80
100
h
Selective film model
Taylor et al.
Original retention curve

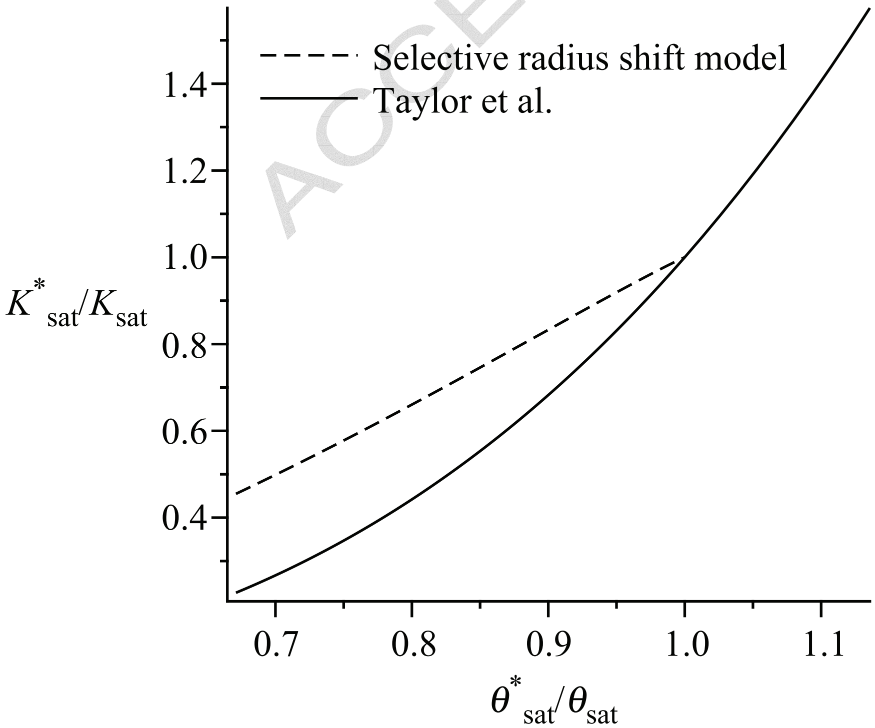
Selective radius shift model
Taylor et al.
1.4
1.2
1.0
0.8
0.6
0.4
K^*_{sat}/K_{sat}
0.7
0.8
0.9
1.0
1.1
$\theta^*_{sat}/\theta_{sat}$

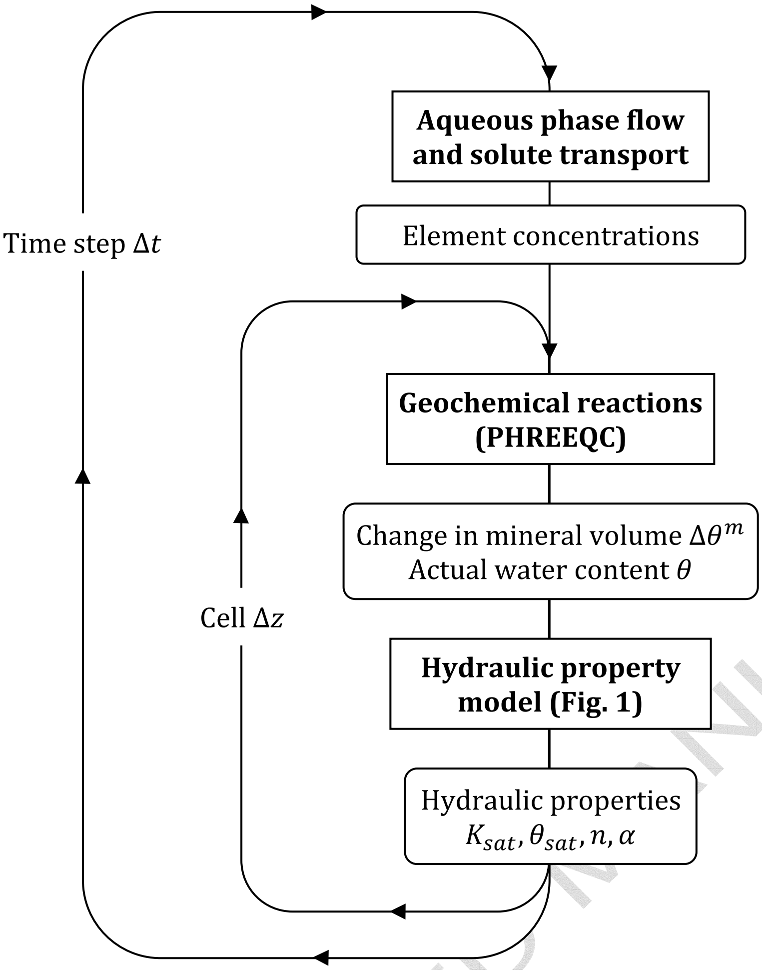
Aqueous phase flow and solute transport
Element concentrations
Geochemical reactions (PHREEQC)
Change in mineral volume $\Delta\theta^m$
Actual water content θ
Hydraulic property model (Fig. 1)
Hydraulic properties
$K_{sat}, \theta_{sat}, n, \alpha$
Time step Δt
Cell Δz

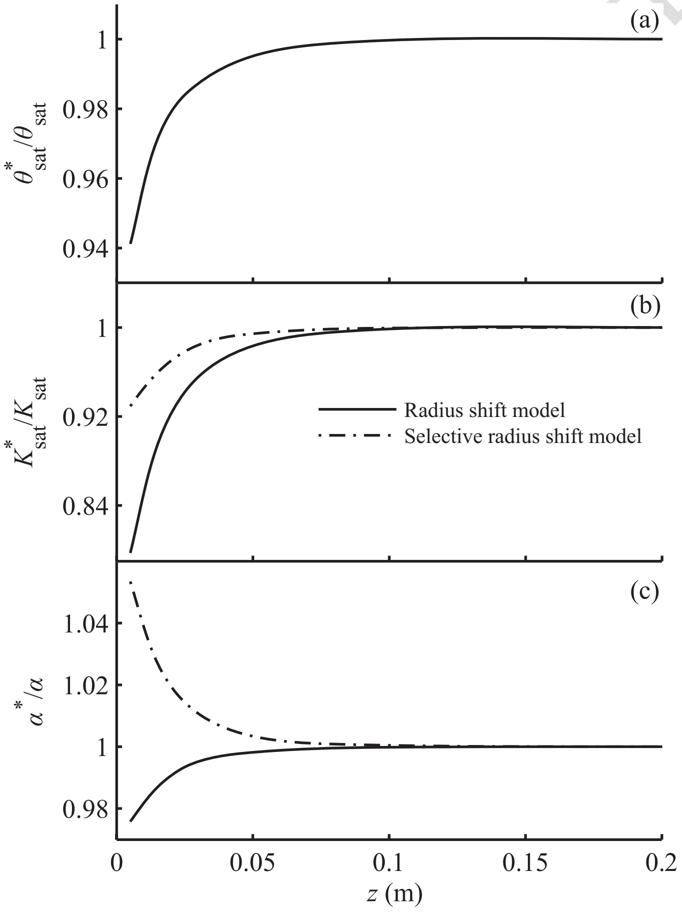
(a)
$\theta^*_{sat}/\theta_{sat}$
1
0.98
0.96
0.94
(b)
K^*_{sat}/K_{sat}
1
0.92
0.84
Radius shift model
Selective radius shift model
(c)
α^*/α
1.04
1.02
1
0.98
0
0.05
0.1
0.15
0.2
z (m)

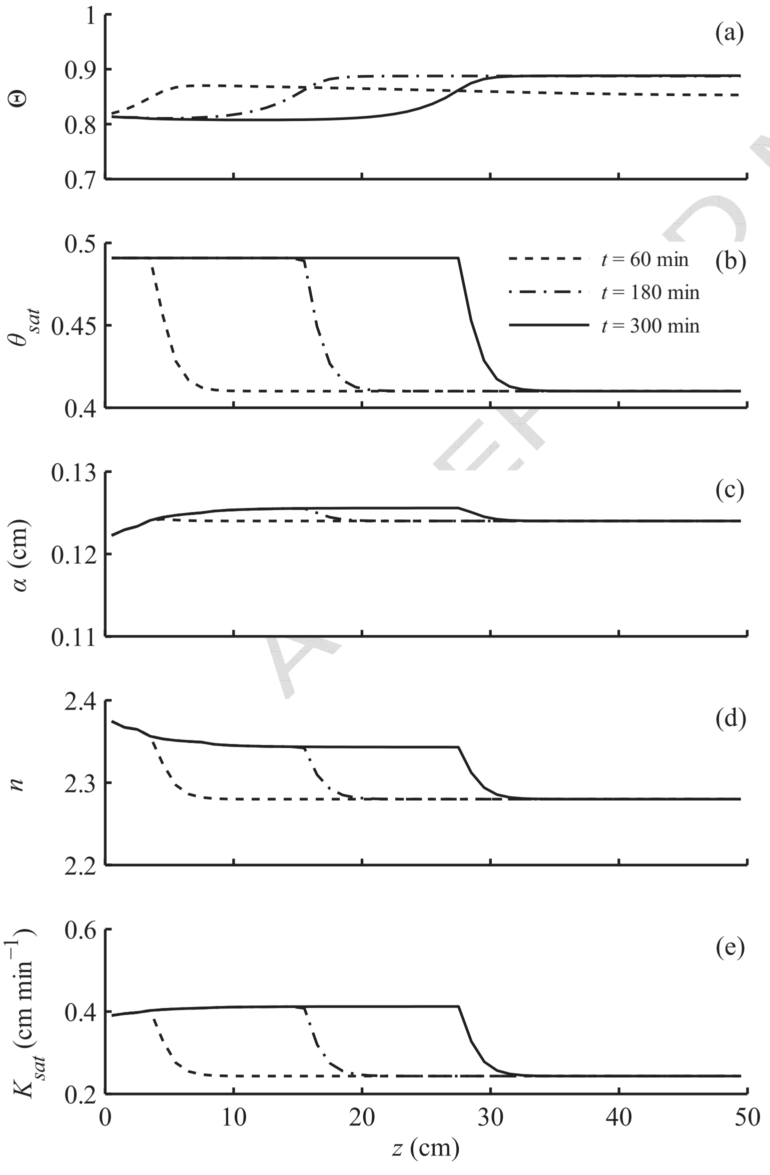

1
0.9
0.8
0.7
Θ
(a)
0.5
0.45
0.4
θ_{sat}
(b)
t = 60 min
t = 180 min
t = 300 min
0.13
0.12
0.11
α (cm)
(c)
2.4
2.3
2.2
n
(d)
0.6
0.4
0.2
K_{sat} (cm min^{-1})
(e)
0
10
20
30
40
50
z (cm)

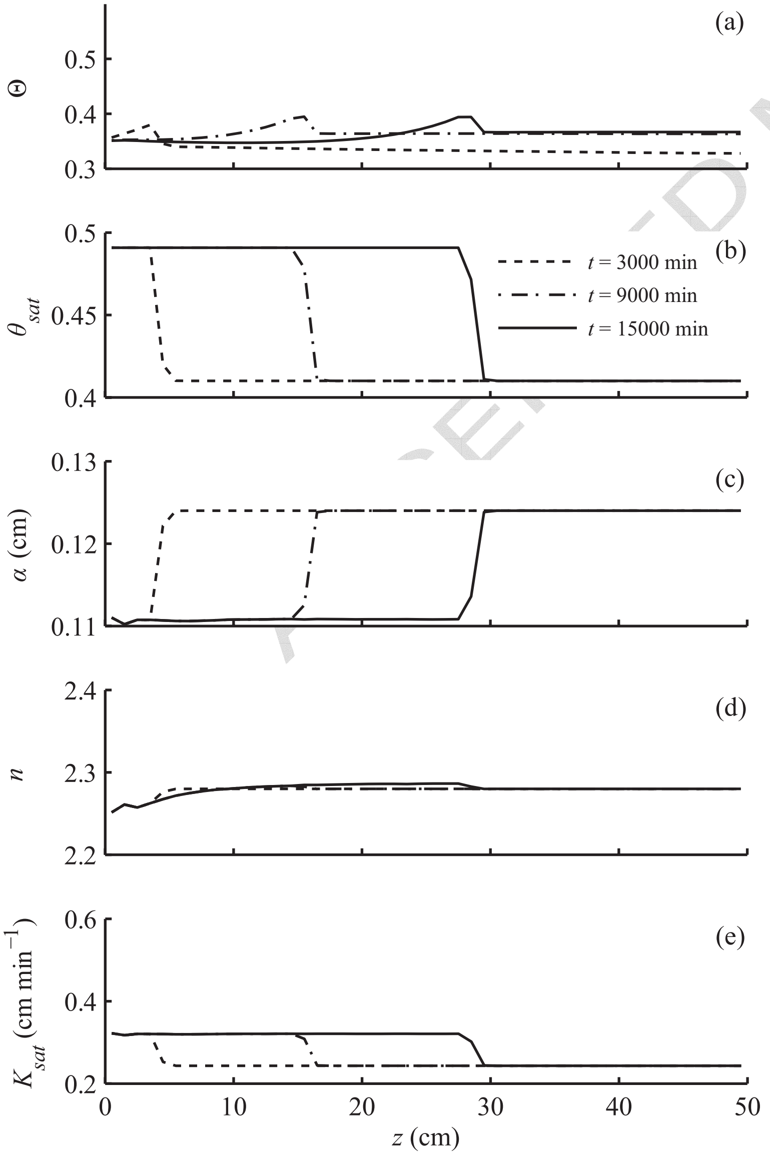
(a)
Θ
0.3
0.4
0.5
(b)
θ_{sat}
0.4
0.45
0.5
t = 3000 min
t = 9000 min
t = 15000 min
(c)
α (cm)
0.11
0.12
0.13
(d)
n
2.2
2.3
2.4
(e)
K_{sat} (cm min^{-1})
0.2
0.4
0.6
0
10
20
30
40
50
z (cm)

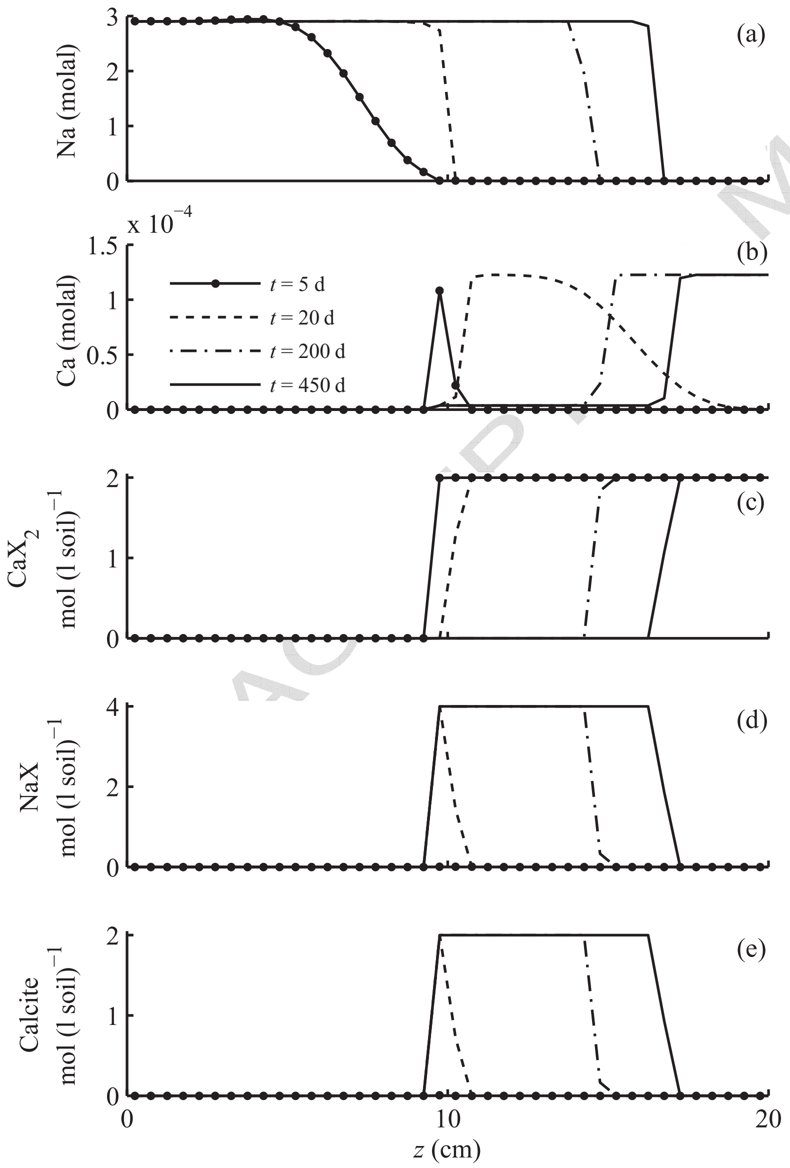
(a)
Na (molal)
3
2
1
0
x 10^{-4}
(b)
Ca (molal)
1.5
1
0.5
0
t = 5 d
t = 20 d
t = 200 d
t = 450 d
(c)
CaX$_2$
mol (l soil)$^{-1}$
2
1
0
(d)
NaX
mol (l soil)$^{-1}$
4
2
0
(e)
Calcite
mol (l soil)$^{-1}$
2
1
0
0
10
20
z (cm)

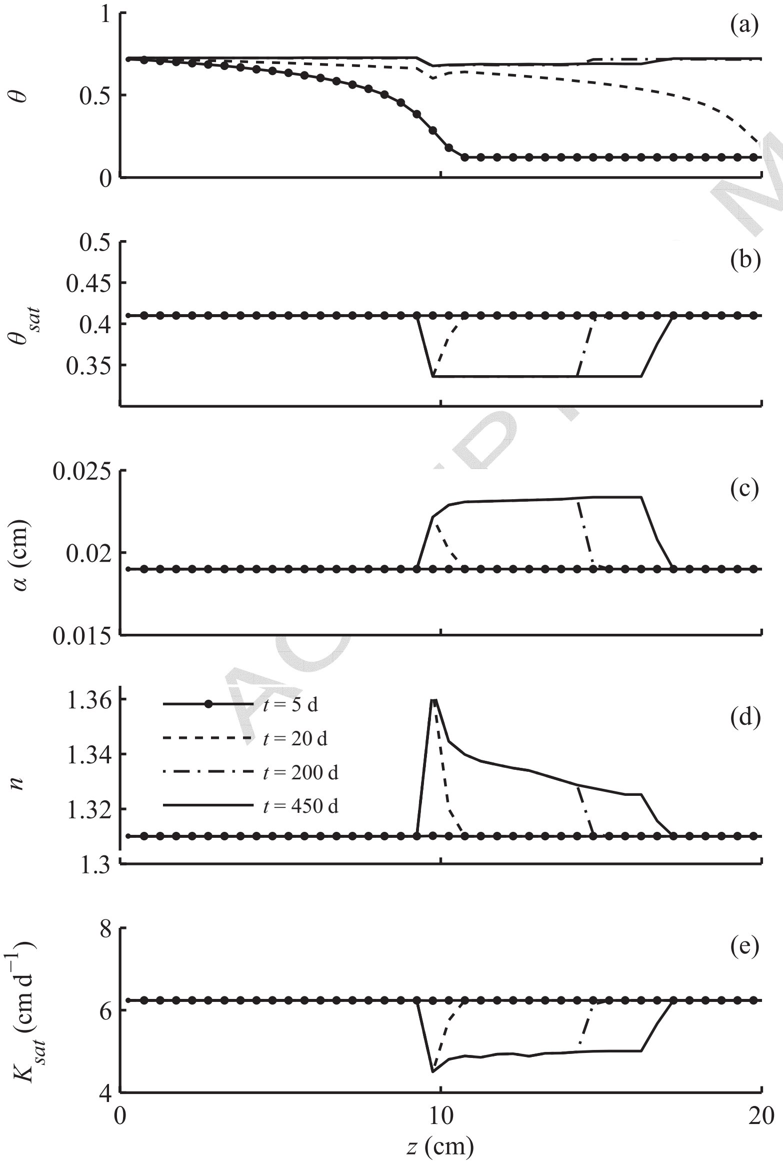
(a)
θ
1
0.5
0
(b)
θ_{sat}
0.5
0.45
0.4
0.35
(c)
α (cm)
0.025
0.02
0.015
(d)
n
1.36
1.34
1.32
1.3
t = 5 d
t = 20 d
t = 200 d
t = 450 d
(e)
K_{sat} (cm d^{-1})
8
6
4
0
10
20
z (cm)

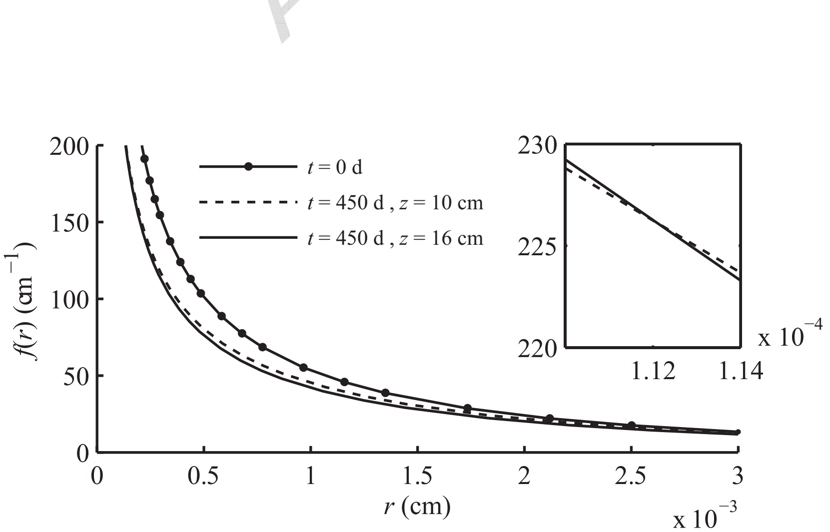
200
150
100
50
0
f(r) (cm^{-1})
0
0.5
1
1.5
2
2.5
3
r (cm)
x 10^{-3}
t = 0 d
t = 450 d , z = 10 cm
t = 450 d , z = 16 cm
230
225
220
1.12
1.14
x 10^{-4}

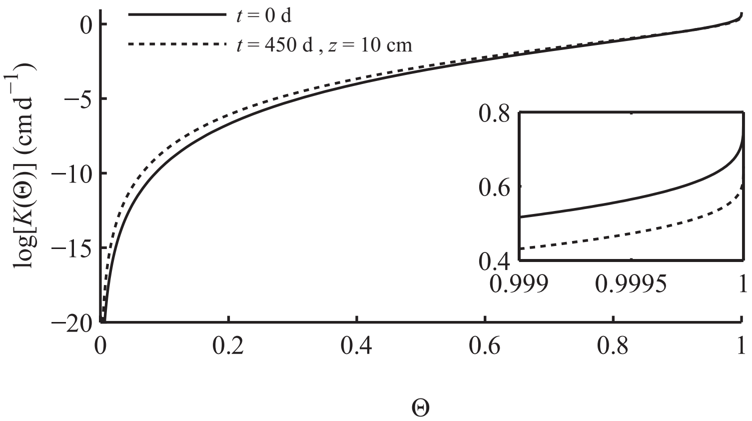
t = 0 d
t = 450 d , z = 10 cm
log[K(Θ)] (cm d^{-1})
0
−5
−10
−15
−20
0
0.2
0.4
0.6
0.8
1
Θ
0.8
0.6
0.4
0.999
0.9995
1